Computers in Biology and Medicine 179 (2024) 108907

Contents lists available at ScienceDirect

Computers in Biology and Medicine

journal homepage: www.elsevier.com/locate/compbiomed

In silico exploration of 4(α-L-rhamnosyloxy)-benzyl isothiocyanate: A promising phytochemical-based drug discovery approach for combating multi-drug resistant *Staphylococcus aureus*

Soham Bhattacharya [a,1], Adrish Dutta [b,1], Pijush Kanti Khanra [c], Neha Gupta [b], Ritesh Dutta [d], Nikolay T. Tzvetkov [e], Luigi Milella [f,*], Maria Ponticelli [e,f]

[a] *Department of Agroecology and Crop Production, Faculty of Agrobiology, Food and Natural Resources, Czech University of Life Sciences Prague, Kamýcká 129, Prague 6, Suchdol, 165 00, Czech Republic*
[b] *Department of Crop Sciences and Agroforestry, Faculty of Tropical AgriSciences, Czech University of Life Sciences Prague, Kamýcká 129, Suchdol, 165 00, Prague 6, Czech Republic*
[c] *Department of Biosciences and Bioengineering, Indian Institute of Technology Guwahati, Guwahati, 39, Assam, India*
[d] *Environmental Biotechnology & Genomics Division, CSIR-National Environmental Engineering Research Institute (CSIR-NEERI), Nehru Marg, Nagpur, 440020, India*
[e] *Department of Biochemical Pharmacology & Drug Design, Institute of Molecular Biology "Roumen Tsanev", Bulgarian Academy of Sciences (BAS), Acad. G. Bonchev Str., Bl. 21, 1113, Sofia, Bulgaria*
[f] *Department of Science, University of Basilicata, Via Dell'Ateneo Lucano 10, 85100, Potenza, Italy*

ARTICLE INFO

Keywords:
Glucomoringin isothiocyanate
GO and KEGG enrichment pathway
In silico pharmacokinetic analysis
Molecular docking
MD simulation
Multi-drug resistance

ABSTRACT

Multidrug-resistant (MDR) *Staphylococcus aureus* infections significantly threaten global health. With rising resistance to current antibiotics and limited solutions, the urgent discovery of new, effective, and affordable antibacterials with low toxicity is imperative to combat diverse MDR *S. aureus* strains. Hence, in this study, we introduce an *in silico* phytochemical-based approach for discovering novel antibacterial agents, underscoring the potential of computational approaches in therapeutic discovery. Glucomoringin Isothiocyanate (GMG-ITC) from *Moringa oleifera* Lam. is one of the phytochemical compounds with several biological activities, including antimicrobial, anti-inflammatory, and antioxidant activities, and is also effective against *S. aureus*. This study focuses on screening GMG-ITC as a potential drug candidate to combat MDR *S. aureus* infections through a molecular docking approach. Moreover, interaction amino acid analysis, *in silico* pharmacokinetics, compound target prediction, pathway enrichment analysis and molecular dynamics (MD) simulations were conducted for further investigation. Molecular docking and interaction analysis showed strong binding affinity towards *S. aureus* lipase, dihydrofolate reductase, and other MDR *S. aureus* proteins, including penicillin-binding protein 2a, MepR, D-Ala: D-Ala ligase, and RPP TetM, through hydrophilic and hydrophobic interactions. GMG-ITC also showed a strong binding affinity to cyclooxygenase-2 and FAD-dependent NAD(P)H oxidase, suggesting that it is a potential anti-inflammatory and antioxidant candidate that may eliminate inflammation and oxidative stress associated with *S. aureus* infections. MD simulations validated the stability of the GMG-ITC molecular interactions determined by molecular docking. *In silico* pharmacokinetic analysis highlights its potency as a drug candidate, showing strong absorption, distribution, and excretion properties in combination with low toxicity. It acts as an active protease and enzyme inhibitor with moderate activity against GPCR ligands, ion channels, nuclear receptor ligands, and kinases. Enrichment analysis further elucidated its involvement in important biological, molecular, and cellular functions with potential therapeutic applications in diseases like cancer, hepatitis B, and influenza. Results suggest that GMG-ITC is an effective antibacterial agent that could treat MDR *S. aureus*-associated infections.

1. Introduction

Antimicrobial resistance (AMR) is one of the most serious threats to

* Corresponding author.
E-mail address: luigi.milella@unibas.it (L. Milella).
[1] Authors sharing the first authorship.

https://doi.org/10.1016/j.compbiomed.2024.108907
Received 4 June 2024; Received in revised form 14 July 2024; Accepted 15 July 2024
Available online 20 July 2024

public health. The abuse and overuse of antimicrobials in humans and animals are the main drivers in developing drug-resistant pathogens. They acquire resistance through various mechanisms, including the prevention of drug entry, expulsion of the drug via active efflux, mutation of targets, and enzymatic inactivation [1]. Bacterial AMR was estimated to be directly responsible for 1.27 million global deaths in 2019 and contributed to 4.95 million deaths [2]. AMR makes infections harder to treat, renders other medical procedures and treatments such as surgery, cesarean sections, and cancer chemotherapy much riskier, and undermines modern medicine ineffective. The World Bank also estimates that AMR could result in US$ 1 trillion in additional healthcare costs by 2050, and US$ 3.4 trillion in gross domestic product (GDP) losses per year by 2030 [3]. The rise in resistance of disease-causing pathogens to antibiotics was reported in 76 countries, which is not bound by any boundaries. Among these, there was a 42 % increase in third-generation cephalosporin-resistant *Escherichia coli* and a 35 % increase in methicillin-resistant *S. aureus* [4]. Given the current arsenal of medications, including methicillin, vancomycin, daptomycin, and linezolid multidrug-resistant *S. aureus* has emerged as the most resistant bacterial strain, representing a significant threat to public health. It is indeed the primary cause of life-threatening infections and diseases in humans, such as nosocomial pneumonia, osteomyelitis, endocarditis, sepsis, and bacteraemia [5,6]. Specifically, MDR *S. aureus* is the predominant isolate responsible for nosocomial infections, exacerbating patient morbidity and mortality rates while imposing significant economic burdens through increased healthcare expenses and prolonged hospitalisations [2].

MDR *S. aureus* strains such as methicillin-resistant *S. aureus* (MRSA), vancomycin-resistant *S. aureus* (VRSA-9), tigecycline-resistant *S. aureus* (TRSA), tetracycline-resistance *S. aureus* (TetRSA), etc. have reported resistance to β-lactam antibiotics, thereby increasing the overall medical costs associated with treatment and posing a huge burden to pharmaceutical industries [7]. MRSA infection is associated with approximately $3 billion in annual healthcare costs and is expected to increase over time [8]. Overuse of antibiotics suppresses susceptible bacteria, increasing the likelihood that resistant bacteria will survive, thus triggering dormant resistance genes in bacteria, which causes bacterial resistance emergence [9]. Due to the decreased susceptibility of MDR *S. aureus* to antibiotics such as methicillin, vancomycin, tetracycline, daptomycin, and linezolid, infections become exceedingly difficult to treat, often resulting in treatment failure and patient death [10,11]. Hence, there is an urgent need for alternative antibacterial to combat MDR *S. aureus* infections. Between these, there are plant-based products that may represent safer options for formulating phytochemical-based drugs to be adopted as a sustainable alternative antimicrobial agent.

Plant-derived secondary metabolites with antibacterial properties represent a promising avenue for designing novel therapeutics. Plant extracts' phytochemicals are the main contributors, offering diverse antimicrobial, anti-inflammatory, antioxidant, antihelmintic, and antiviral properties. These properties make secondary metabolites effective, economical, and low in toxicity [12]. In particular, several studies have shown that phytochemicals obtained from medicinal plants belonging to different classes, such as coumarins, sterols, triterpenes, carbazole alkaloids, pypayafoline, triterpenoid, alkaloids, flavonoids, and phenolic acids have immense potential to inhibit the growth of MDR strains [13–15].

Moringa oleifera Lam. is a medicinal plant composed of diverse phytochemicals like moringin, glucomoringin, glucotropaeolin, palmitic acid, quercetin, kaempferol, isorhamnetin, and others. The leaves, seeds, pods, flowers, roots, and bark extracts of *Moringa oleifera* Lam. are rich in several alkaloids, saponins, terpenoids, flavonoids, etc., and demonstrate potent antibacterial activity against multidrug-resistant *S. aureus* [16,17]. Additionally, these compounds offer various pharmaceutical properties, including antioxidant, anti-inflammatory, antidiabetic, and antimicrobial activities [18,19].

Among the phytochemicals found in *M. oleifera,* there is a growing interest in exploring (α-L-rhamnosyloxy)-benzyl isothiocyanate (glucomoringin isothiocyanate; GMG-ITC) from *M. oleifera* seeds. It is released by the catalyzed hydrolysis of 4 (α-L-rhamnosyloxy)-benzyl glucosinolate (glucomoringin; GMG) by myrosinase (Fig. 1) [20,21]. GMG-ITC has been reported to have a variety of biological activities, including antimicrobial, anti-inflammatory, antioxidant, and anti-ulcer [22], as well as antibacterial activity against *S. aureus* and various MDR bacteria such as *S. aureus*, *E. coli*, and *Pseudomonas aeruginosa* [23]. However, its probable bacterial drug targets and their molecular interactions with target proteins have not yet been elucidated. There is thus an urgent need to explore GMG-ITC as a probable drug candidate against MDR *S. aureus*. Therefore, this study aims to investigate GMG-ITC's potential as an antibacterial drug against MDR *S. aureus*. The present investigation explores the molecular interactions of GMG-ITC with bacterial targets, analyses the pharmacokinetics, evaluates potential human targets, and investigates the interaction of GMG-ITC with metabolic pathways to establish it as a promising drug candidate (Fig. 2).

Abbreviations

AMR	Antimicrobial resistance
BPs	Biological processes
CC	Cellular component
CYP	Cytochrome P450
GO	Gene Ontology
GMG	Glucomoringin
GMG-ITC	Glucomoringin Isothiocyanate
GDP	Gross domestic product
hERG	Human ether-a-go-go-related gene
HB	Hydrogen bond
HYDE	HYdrogen Desolvation
ICM	Ion channel modulator
KI	Kinase inhibitor
KEGG	Kyoto Encyclopedia of Genes and Genomes
Ro5	Lipinski's rules of five
MRTD	Maximum Recommended Tolerance Dose
MRSA	Methicillin-resistant *S. aureus*
MD	Molecular dynamics
MFs	Molecular functions
MDR	Multidrug-resistant
NRL	Nuclear receptor ligand
OCT2	Organic cation transporter 2
Rg	Radius of gyration
RMSD	Root-mean-square deviation
RMSF	Root-mean-square fluctuation
SAL	*S. aureus* lipase
SASA	Solvent accessible surface area
VDss	Steady-state volume of distribution
TetRSA	Tetracycline-resistance *S. aureus*
TRSA	Tigecycline-resistant *S. aureus*
TPSA	Topological polar surface area
VRSA-9	Vancomycin-resistant *S. aureus*

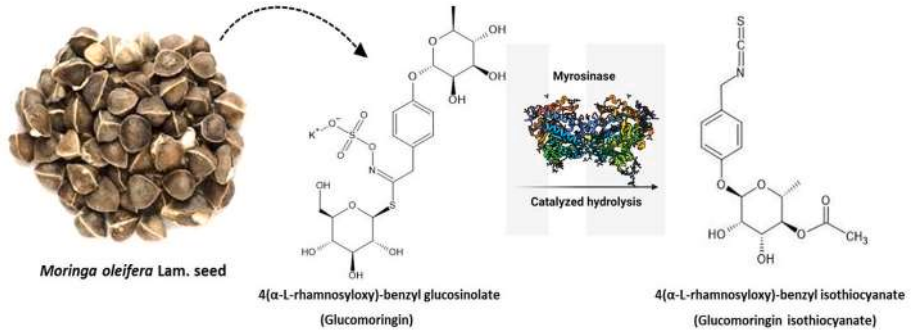

Fig. 1. A schematic diagram showing the purification of GMG-ITC from GMG through catalyzed hydrolysis by myrosinase enzyme.

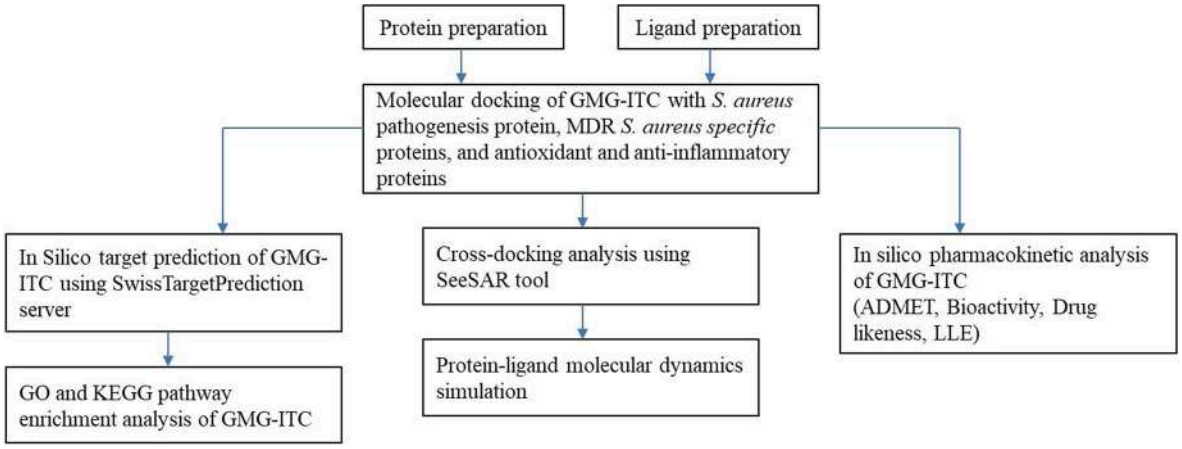

Fig. 2. Schematic diagram of the workflow.

2. Material and methods

2.1. Target protein identification

To explore the best phytochemical-based drug against MDR *S. aureus* it is essential to identify the probable molecular drug targets. For that, proteins that are mainly involved in *S. aureus* pathogenesis such as V8 protease (PDB ID: 2O8L) [24], Signal Transduction Protein Trap (PDB ID: 4AE5) and *S. aureus* lipase (PDB ID: 6KSI) [25], as well as several universal bacterial proteins were identified as described by Jianu et al. (2021) [26]. In addition, resistant bacteria-specific target proteins such as beta-lactamase (PDB ID: 1GHI) and penicillin-binding protein 2a (PDB ID: 1MWU) for methicillin-resistant *S. aureus* [27], Tet repressor protein (PDB ID: 2FJ1), RPP TetM in complex with 70 S ribosome (PDB ID: 3J25) [28] and QacA antiporter protein (PDB ID: 7Y58) for tetracycline-resistant *S. aureus* [29], MepR transcription regulator (PDB ID: 3ECO) for tigecycline-resistant *S. aureus* [30], D-Ala:D-Ala ligase (PDB ID: 3N8D) for vancomycin-resistant *S. aureus* [31] were used as input 3D protein structures. Also, to check the bioactivity of the phytochemical, several proteins involved in antioxidant and anti-inflammatory activity such as cyclooxygenase-2 (PDB ID: 1CX2), Lipoxygenase with protocatechuic acid (PDB ID: 1N8Q), hyaluronidase (PDB ID: 2PE4), Lipoxygenase (PDB ID: 3V92), inducible nitric oxide synthase (PDB ID: 4CX7) and 11β-hydroxysteroid dehydrogenase 1 (PDB ID: 4YYZ) were also investigated. Whereas the proteins for oxidative activities were human cyclin-dependent kinase 2 complex (PDB ID: 1HCK), FAD-dependent NAD(P)H oxidase (PDB ID: 2CDU), glutathione peroxidase (PDB ID: 2F8A) and superoxide dismutase (PDB ID: 3HFF).

2.2. Target and ligand preparation

The crystal structures of all the above-mentioned proteins were retrieved from RCSB PDB database (https://www.rcsb.org/, accessed on March 12, 2024) and used throughout the study. For docking studies, the unwanted chains and residues present in the proteins were removed using UCSF Chimera ver. 1.16 (https://www.rbvi.ucsf.edu/chimera).

The 3D SDF structure of glucomoringin isothiocyanate (GMG-ITC), the active component of *M. oleifera* seeds extracts previously reported to exhibit good antibacterial activity, was downloaded from the PubChem database (https://pubchem.ncbi.nlm.nih.gov/, accessed on March 12, 2024). Along with GMG-ITC, the 3D SDF structures of control compounds such as ascorbic acid [32], ibuprofen [33], and 2-oxazolidinone [34] were also retrieved. All compounds were imported into Avogadro software version 1.2.0 and exposed to energy minimization. The energy minimization was accomplished with the MMFF94 force field using the steepest descent algorithm. The structures were further converted to the PDBQT format for docking.

2.3. Molecular docking and interaction analysis

Molecular docking was conducted to understand the interaction and binding affinity between phytochemicals and bacterial protein receptors, while also validating their antioxidant and anti-inflammatory properties. The docking study was performed in two steps (primary and final screening) using a command Prompt with all the information from AutoDock Tools as described by Gupta et al. (2023) [35] with slight modifications. In primary screening, the GMG-ITC compound was pre-screened with the proteins involved in the *S. aureus* pathogenesis. The compound was then further docked with all the proteins taken in this study to perform final docking studies, simulations, and other

analyses. The obtained protein-ligand complexes were visualized and analyzed by BIOVIA Discovery Studio Visualizer (BIOVIA, San Diego, CA, USA). The follow-up detailed analysis of the respective amino acid residue-ligand interaction was also performed using the same software tool. The compounds with the best binding affinity values, targeting the proteins used in the study, were selected for further molecular dynamics simulation analysis.

2.4. Crosschecking docking and interaction of the ligands with proteins

For crosschecking the binding affinities of GMG-ITC with selected proteins, online docking was performed using the CB-Dock2 online server (https://cadd.labshare.cn/cb-dock2/index.php, accessed on March 12, 2024).

2.5. Cross-docking and HYDE analysis

Cross-docking and subsequent HYdrogen DEsolvation (HYDE) analysis of GMG-ITC with selected eight proteins were performed using the SeeSAR v.13.1 (www.biosolveit.de, BioSoveIT GmbH, St. Augustin, Germany, 2024). The docking module implemented in SeeSAR and the integrated scoring function HYDE have been performed using a standard docking procedure with the 3D structure of GMG-ITC and protein as obtained from the initial docking experiments (cf. Experimental part 2.3). The best-ranked docking poses were visually inspected and selected, if necessary, for further computing in terms of optimization of torsions/bindings and intra-/intermolecular clashes by using the molecular editor module in SeeSAR with subsequent re-docking and -scoring [36]. As integrated in SeeSAR, the HYDE scoring function considers the hydrogen/salt bridges bonds (usually interpreted as the enthalpy term ΔH) and dehydration term (interpreted as the entropy –TΔS) based on the contribution of all non-hydrogen (heavy) atoms for both ligand and protein to the overall free energy of binding (ΔG, kJ/mol) [37]. As a result, HYDE rapidly computes the predicted binding affinities (ΔG) in the form of so-called $K_{i\ HYDE}$ ranges (including lower and upper $K_{i\ HYDE}$ boundaries) as well as other relevant drug-like properties like LE/LLE_{HYDE}, logP/D, and others.

2.6. In silico pharmacokinetics, drug-likeness, and bioactivity analysis

Pharmacokinetics parameters related to absorption, distribution, metabolism, excretion, and toxicity (ADMET) play a substantial role in identifying novel drug candidates. To predict the pharmacokinetics of the candidate molecules, pkCSM (https://biosig.lab.uq.edu.au/pkcsm/prediction, accessed on March 12, 2024) online tool was used. Parameters such as AMES properties, maximum tolerated dose (human), hERG inhibitory effects, oral rat acute and chronic toxicities, hepatotoxicity, skin sensitization, fathead minnow toxicity, aqueous solubility scale, blood-brain barrier permeability, CYP inhibitory activity, and total clearance were also explored.

In addition to these, molecular properties of top hit compounds such as molecular weight, hydrogen bond acceptor, hydrogen bond donor, number of rotatable bonds, topological polar surface area, octanol/water partition coefficient, and Lipinski's rule of five were also evaluated and were obtained from SwissADME (http://www.swissadme.ch/, accessed on March 18, 2024). The bioactivity scores of ligands against regular human receptors such as GPCRs, ion channels, kinases, nuclear receptors, proteases, and enzymes were assessed by the molinspiration web server (https://www.molinspiration.com/cgi/properties, accessed on March 18, 2024).

2.7. In silico target prediction

The selected ligand GMG-ITC was used for target prediction on a SwissTargetPrediction server (http://www.swisstargetprediction.ch/, accessed on March 18, 2024), Utilizing its predictive algorithms, potential protein targets for the compounds were identified based on structural and chemical similarities [38], where *Homo Sapiens* was designated as the target organism as previously performed by Daina et al. (2019) [39].

2.8. GO and KEGG pathway analysis

The predicted target data were subjected to Gene Ontology (GO) analysis to screen for involvement in biological processes (BPs), cellular components (CCs), and molecular functions (MFs). While Kyoto Encyclopedia of Genes and Genomes (KEGG) enrichment analysis identified critical signalling pathways associated with these biological processes were collected from the DAVID database (https://david.ncifcrf.gov/, accessed on April 27, 2024) to elucidate the roles of the target proteins in gene function and signalling pathways. This combined analysis provided comprehensive insights into the functional diversity and molecular mechanisms underlying the effects of the compounds [40]. Subsequently, the GO was uploaded to the Bioinformatics platform (http://www.bioinformatics.com.cn/, accessed on April 27, 2024) for visualization, according to Liu et al. (2024) [41]. KEGG data was obtained and visualized from ShinyGO (http://bioinformatics.sdstate.edu/go77/) for further analysis as described by Bodnár et al. (2024) [42]. Statistical methods, including *p*-value calculation and correction for multiple testing, were applied to ensure the robustness of the results [43].

2.9. Protein-ligand molecular dynamics simulation

The six best protein-ligand complexes with tested compounds were obtained from the molecular docking study for MD simulation based on the lowest binding energy achieved along with the optimal docked pose. In this study, we have generated a comparison analysis map based on the dynamic characteristics of our targeted proteins along with their interactive protein-ligand complexes using GROMACS 2019.1 tool. In this investigation, Molecular Dynamics Simulations (MDS) of protein-ligand complexes were conducted employing the CHARMM36 force field (http://www.charmm-gui.org/) within GROMACS version 2019.1. The parameter files for the chosen docked complexes were prepared following the guidelines provided in the GROMACS tutorial. The topology and parameter files for each protein and ligand were generated on the CHARMM-GUI server and further selected protein-ligand complex file preparation has been done via CHARMM-GUI Multicomponent Assembler (MCA). The length of each side of the cube enclosing the system was determined based on parameters such as "Calculated Volume Fraction", "Minimum Recommended Size Length", and "Maximum Volume Fraction", ensuring a minimum of 20 Å increase in the "Box XYZ length (Å)" to mitigate risks of periodic image atoms crossing system boundaries during MD simulation. Guided the system size in the last step, the solvent composition was automatically calculated, and the system was solvated by TIP3P water molecules and K^+, Cl^- ions (at a concentration of 150 mM) similarly as per the guided protocol of Solution Builder. Gromacs files specific to proteins, and protein-ligand complexes have been extracted from generated chrmm-gui files for targeted MD run for 100 ns (nanoseconds) with 2 fs (fs) steps.

2.10. MD run post-analysis

MD trajectory analysis is a comparison analysis to compare the stability and strength of protein-ligand complexes for proteins based on some topological parameters root-mean-square deviation (RMSD), root-mean-square fluctuation (RMSF), solvent accessible surface area (SASA), radius of gyration (R_g), Coul-SR energy, LJ-SR energy, and hydrogen bond (HB) formation. All those graphs (RMSD, RMSF, SASA, R_g, HB, Coul-SR, and LJ-SR energy) were plotted by using Qtgrace (https://qtgrace.sourceforge.io/) with the aid of extracted data achieved by the successive run of GROMACS commands ("gmx rms", "gmx rmsf", "gmx

hbond", "gmx SASA", "gmx gyrate", "gmx energy"). Finally, "gmx trjconv" command of the GROMACS tutorial was run for extraction of specific protein-ligand interaction complexes with a time interval of 20 ns throughout the whole 100 ns of MD trajectory.

3. Results

3.1. Molecular docking analysis

To identify a potential phytochemical-based drug against MDR *S. aureus*, a molecular docking approach was performed with GMG-ITC. Initially, GMG-ITC was docked with pathogenesis-causing proteins of *S. aureus* for primary screening (Table 1), followed by further analysis with all selected proteins (Fig. S1). The binding energies of all selected proteins with GMG-ITC and reference drugs are listed in Table 1. GMG-ITC exhibited good binding affinities of more than −4.5 kcal/mol with all the proteins used in the study, ranging from −7.6 kcal/mol to −4.7 kcal/mol. Notably, the compound had the strongest binding affinity (−7.3 kcal/mol) to *S. aureus* lipase (PDB ID: 6KSI) compared to other pathogenic proteins tested in this study, forming hydrogen bond with a bond length of 4.14 Å with A chain's amino acid Leu18, along with various other non-weak interactions with A chain's amino acid residues His115, His349, Phe17, Val309, and Val350 (Fig. 3A–B). Additionally, the tested compound exhibited a binding affinity of −7.8 kcal/mol with dihydrofolate reductase (PDB ID: 3SRW), which is essential for bacterial DNA synthesis. In this case, a hydrogen bond (bond length of 5.31 Å) with Asp28 and other interactions with Asp28, His31, Ile15, Ser50, and Thr47 were observed (Fig. 3C–D). In MRSA, penicillin-binding protein 2a (PDB ID: 1MWU) confers broad-spectrum beta-lactam resistance. The binding of PBPs with an inhibitor disrupts peptidoglycan cross-linking, hindering cell wall synthesis. Within the protein-ligand complex with 1MWU, GMG-ITC showed a strong binding affinity with a binding energy of −6.8 kcal/mol that involved three hydrogen bond interactions with lengths of 4.52 Å, 5.45 Å, and 4.04 Å for Arg241, His293, and Thr165, respectively, along with other non-weak interactions with Asp275, Asp295, His293, Val256, and Val277 (Fig. 4A–B). Similarly, in VRSA-9, D-Ala:D-Ala ligase (PDB ID: 3N8D) is pivotal for ligase impairment, while MepR transcription regulator (PDB ID: 3ECO) mediates tigecycline resistance by suppressing the multi-drug efflux pump gene. Additionally, RPP TetM (PDB ID: 3J25) in complex with the 70 S ribosome contributes to tetracycline resistance by mutating domain IV's interaction point with the tetracycline binding site. These proteins can be considered as probable drug targets for an effective strategy against VRSA-9, TRSA, and TetRSA. GMG-ITC showed good binding interactions (Fig. 4) with all of these proteins with a binding energy of −7.5 kcal/mol, −5.9 kcal/mol, and −7.4 kcal/mol, respectively, compared to the reference antibiotic 2-oxazolidinone which is an effective drug against all these bacterial strains.

Further, to check the anti-inflammatory and antioxidant activity of GMG-ITC, it was docked with the molecular targets responsible for the anti-inflammatory and antioxidant activity in the human body. The investigated compound exhibited the highest binding affinity for cyclooxygenase-2 (PDB ID: 1CX2) (−7.1 kcal/mol) compared to the reference anti-inflammatory drug ibuprofen with the interaction of two hydrogen bonds of length 4.98 Å and 5.09 Å with Asn382 and other interactions with Glu290, His214, His386, Thr212, and Val291 (Fig. 5A–B). FAD-dependent NAD(P)H oxidase (PDB ID: 2CDU), which catalyzes the oxidation of 2 equivalents of either NADH or NADPH, was found to have a good binding affinity with GMG-ITC (−7.6 kcal/mol). The interaction involved two hydrogen bonds with lengths of 4.69 Å and 4.45 Å with Lys134 and Ser41, respectively, while other interactions involved were with Ala300, Ile160, Gly158, and Lys134 (Fig. 5C–D). All the top-hit docking and their interactions are illustrated in Table S1.

To estimate the binding affinity of GMG-ITC towards eight biological

Table 1
Binding free-energy values (ΔG in kcal/mol) of GMG-ITC as a target ligand along with ascorbic acid, ibuprofen, and 2-oxazolidinone as references for good antioxidant, anti-inflammatory, and antibacterial agents, respectively.

Molecular targets	PBD entry	Ligands			
		GMG-ITC	Ascorbic acid	Ibuprofen	2-Oxazolidinone
Anti-inflammatory	4YYZ	−6.3	–	−6.2	–
	1N8Q	−6.9	–	−7.7	–
	2PE4	−6.9	–	−6.2	–
	3V92	−7	–	−6.3	–
	4CX7	6.8	–	−5.7	–
	1CX2	−7.1	–	−6.4	–
Antioxidant	1HCK	−5.9	−4.8	–	–
	2CDU	−7.6	−5.4	–	–
	2F8A	−5.4	−4.4	–	–
	3HFF	−4.7	−4.1	–	–
***S. aureus* pathogenesis**	2O8L	−6.5	–	–	−3.4
	4AE5	−5.9	–		−3
	6KSI	−7.3	–	–	−3.9
Universal bacterial target	1JZQ	−7.2	–	–	−3.6
	1KZN	−5.3	–	–	−3.7
	2VEG	−5.8	–	–	−3.9
	2ZDQ	−5.4	–	–	−3.9
	3RAE	−6.3	–	–	−4
	3SRW	−7.1	–	–	−3.7
	3UDI	−6.2	–	–	−3.5
	3TTZ	−5.9	–	–	−3.3
MRSA	1GHI	−5.6	–	–	−3.3
	1MWU	−6.8	–	–	−3.6
VRSA-9	3N8D	−7.5	–	–	−3.9
TRSA	3ECO	−5.9	–	–	−3.6
TetRSA	2FJ1	−6.4	–	–	−3.5
	3J25	−7.4	–	–	−3.3
	7Y58	−6.6	–	–	−3.7

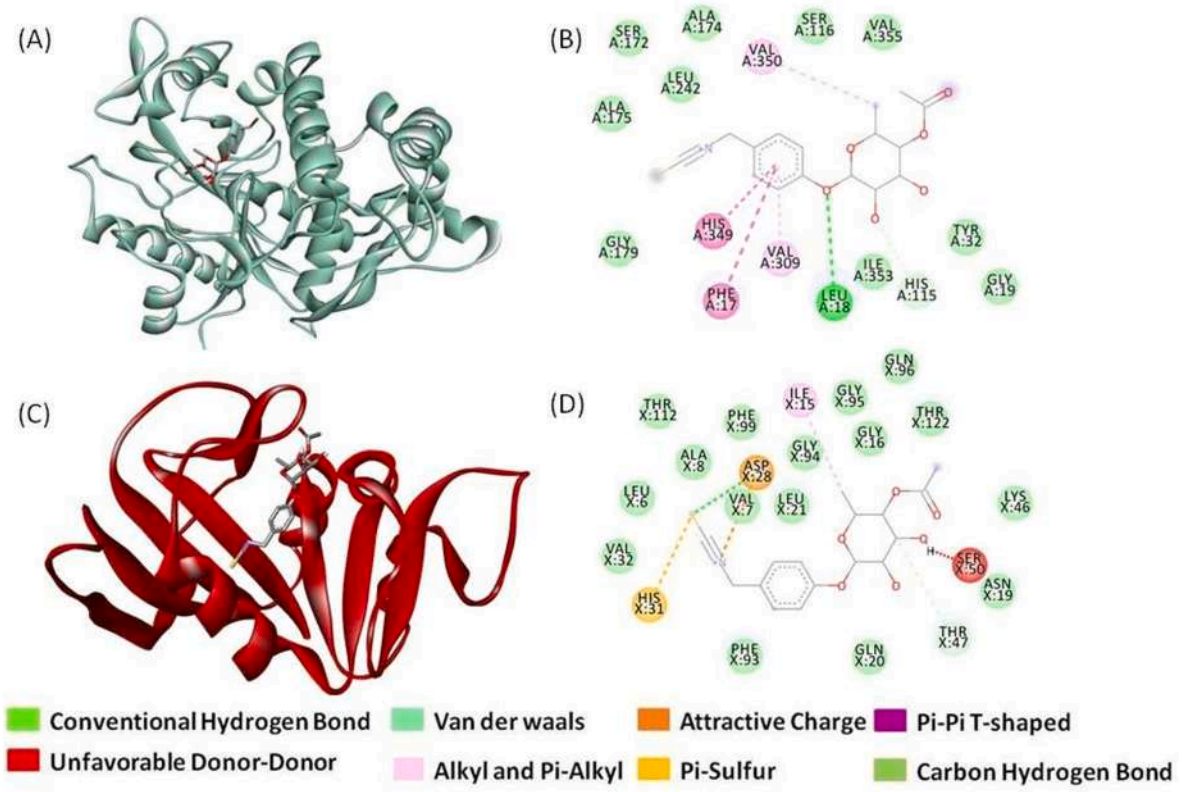

Fig. 3. 3D and 2D interactions of GMG-ITC as ligand with (A) and (B) *S. aureus* lipase (PDB ID: 6KSI), and (C) and (D) Dihydrofolate reductase (PDB ID: 3SRW) as proteins.

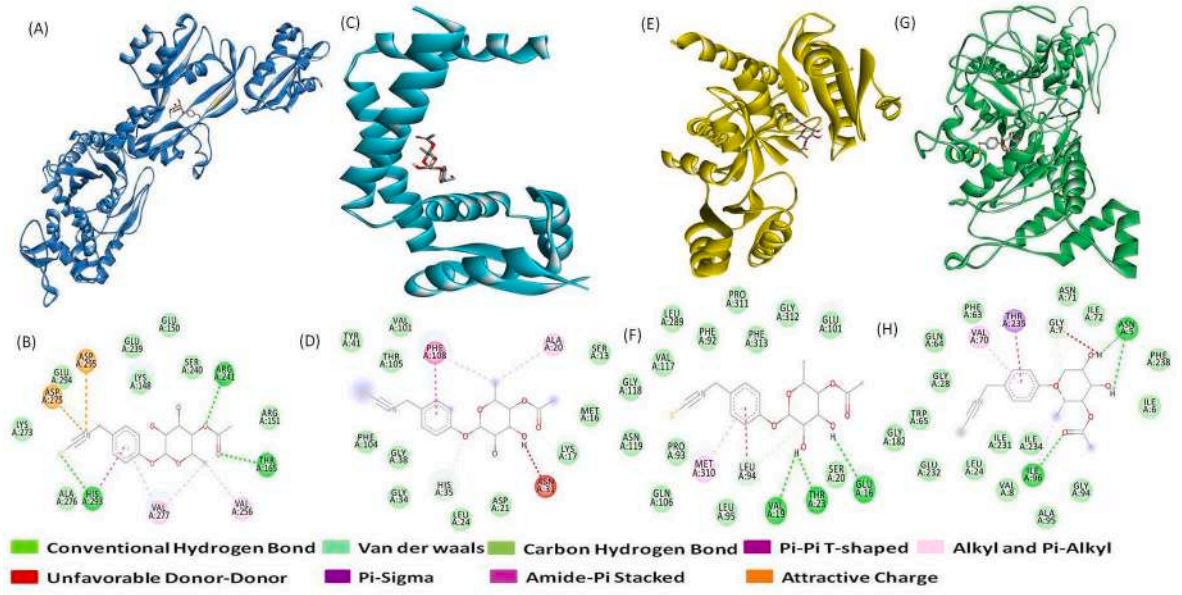

Fig. 4. 3D and 2D interactions of GMG-ITC as ligand with (A) and (B) penicillin-binding protein 2a (PDB ID: 1MWU), (C) and (D) MepR transcription regulator (PDB ID: 3ECO), (E) and (F) D-Ala:D-Ala ligase (PDB ID: 3N8D), and (G) and (H) RPP TetM in complex with the 70 S ribosome (PDB ID: 3J25) as proteins.

targets and quantify our docking results, we performed additional cross-docking analysis using the SeeSAR tool with subsequent HYDE analysis. The implemented HYDE algorithm considers the contribution of all non-hydrogen atoms to the overall binding energy (ΔG, kcal/mol) for both ligand and protein. Therefore, we obtained the so-called $K_{i\ HYDE}$ lower boundaries (from nM to μM ranges). Compared to other proteins tested in this study, GMG-ITC showed the highest binding activity against VRSA-9-9 D-Ala:D-Ala ligase (PDB ID: 3N8D, ΔG = −7.5 kcal/mol, Ki HYDE = 0.293 μM). It also demonstrated strong binding affinity to *S. aureus* lipase (PDB ID: 6KSI, ΔG = −7.3 kcal/mol, Ki HYDE = 0.458 μM), cyclooxygenase-2 (PDB ID: 1CX2, ΔG = −7.1 kcal/mol, Ki HYDE = 0.635 μM), and dihydrofolate reductase (PDB ID: 3SRW, ΔG = −7.1 kcal/mol, Ki HYDE = 0.639 μM). Table S2 summarizes the estimated *K*i HYDE lower boundary values for GMG-ITC against the eight selected

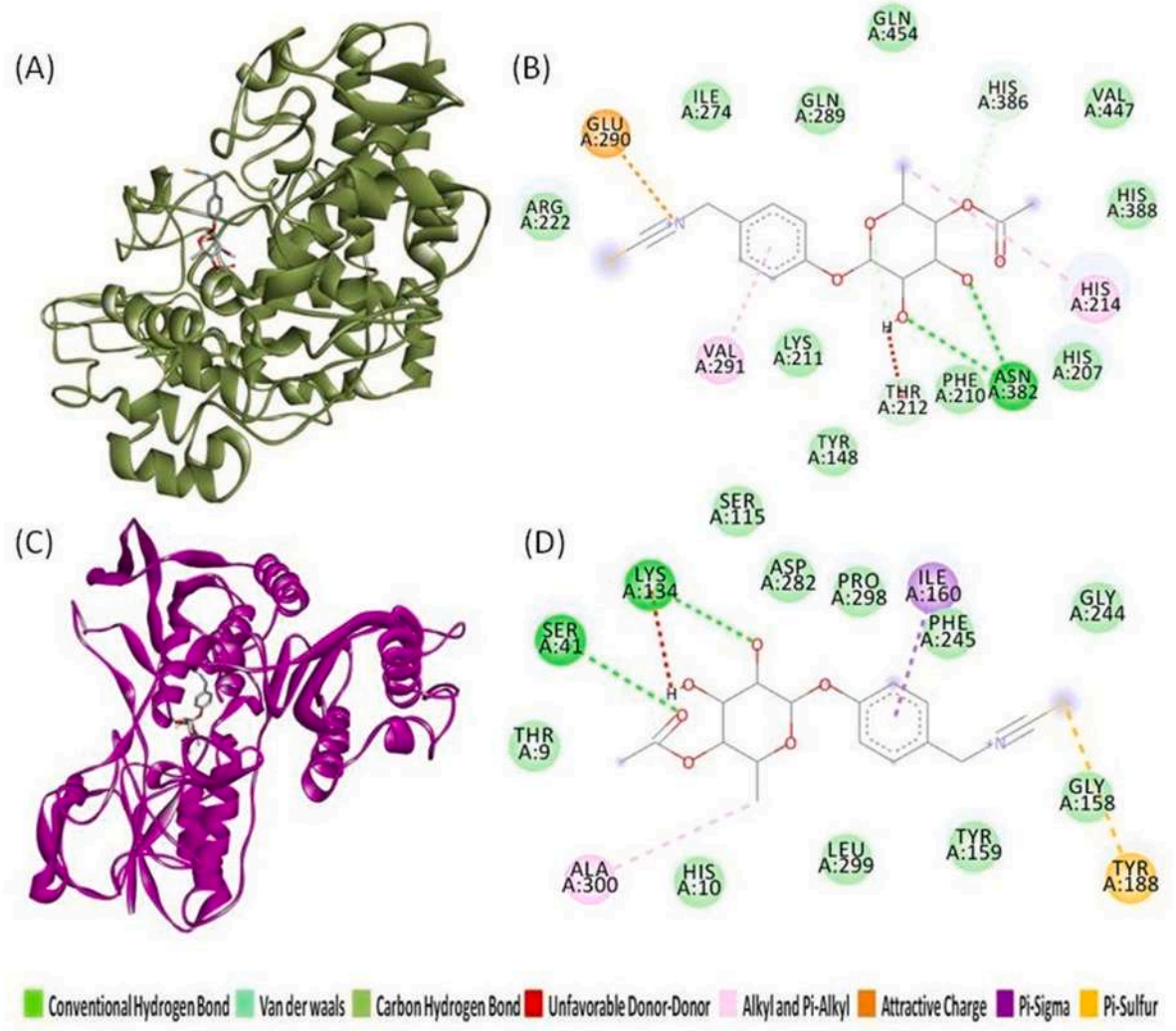

Fig. 5. 3D and 2D interactions of GMG-ITC as ligand with (A) and (B) cyclooxygenase-2 (PDB ID: 1CX2), and (C) and (D) FAD-dependent NAD(P)H oxidase (PDB ID: 2CDU) as proteins.

biological targets based on the docking score. In general, the cross-docking experiments using the HYDE algorithm in SeeSAR produced results consistent with the initial docking studies for the same GMG-ITC–protein complexes (*cf.* Table 1 and Table S2). In addition, we calculated the ligand lipophilicity efficiency (LLE) coefficients for GMG-ITC using SeeSAR. LLE is an important metric in drug design used to improve the lead structure optimization process [44]. In particular, LLE is a measure of the relationship between the *in vitro* (or *in silico* predicted) binding potency of a ligand toward a target of interest and the lipophilicity (measured or calculated partition/distribution coefficient, logP/D) [44]. A compound with a LLE value higher than 5.0 can be considered for further drug optimization. As a part of our investigations, we estimated the LLE values for the selected eight GMG-ITC–protein complexes (cf. Table S2). Therefore, the highest LLE values were found for the highest binding affinities of GMG-ITC to *S. aureus* VRSA-9-9 D-Ala:D-Ala ligase (LLE = 6.02), *S. aureus* lipase (LLE = 5.82), the cyclooxygenase-2 (LLE = 5.69), and dihydrofolate reductase (LLE = 5.68) showing that GMG-ITC exhibit optimal drug-like properties when taking into account its affinity against these proteins.

3.2. Pharmacokinetic analysis

Based on the docking study, GMG-ITC was selected for further pharmacokinetic analysis, including ADMET, Lipinski's rule of five, bioactivity score, and drug-likeness analysis.

3.3. Absorption, distribution, metabolism, excretion, and toxicity (ADMET) analysis

Absorption of drug compounds is mainly analyzed through aqueous solubility, Caco-2 permeability, gastrointestinal absorption in humans, skin permeability, and whether the molecule acts as a substrate or inhibitor of P-glycoprotein. All the parameters for GMG-ITC are included in Table 2. The results obtained indicated that GMG-ITC is moderately soluble in water, whereas the reference drug 2-oxazolidinone showed the highest solubility. Similarly, Caco-2 permeability and human intestinal absorption play crucial roles in determining definitive bioavailability. According to Chandra et al. (2021) [45], a drug compound with a value exceeding 0.90 of Caco-2 permeability is deemed readily permeable. In the present investigation, it was seen that the reference drugs ibuprofen and 2-oxazolidinone are highly permeable, while GMG-ITC showed moderate permeability. According to Saha et al. (2021) [46], the human intestine is mostly an active site for drug absorption, and more than 30 % absorption is considered readily absorbed. The absorption analysis showed that all compounds, including reference drugs, have high absorbance rates in the human intestine, with more than 60 % for GMG-ITC and more than 90 % for the rest of the compounds. The results obtained herein also showed that all investigated

Table 2
Predicted ADMET pharmacokinetic properties.

Property	Model name	Compounds		
		GMG-ITC	Ibuprofen	2-Oxazolidinone
Absorption	Water solubility (log mol/L)	−3.147	−3.696	0.243
	Caco2 permeability (log Papp in 10^{-6} cm/s)	0.604	1.729	1.582
	GI absorption (%)	64.625	94.064	98.901
	P-glycoprotein substrate	No	No	No
	P-glycoprotein I inhibitor	No	No	No
	P-glycoprotein II inhibitor	No	No	No
Distribution	VDss (human) (log L/kg)	−0.379	−0.803	−0.092
	Fraction unbound (human)	0.352	0.239	0.813
Metabolism	CYP2D6 substrate	No	No	No
	CYP3A4 substrate	Yes	No	No
	CYP1A2 inhibitor	No	No	No
	CYP2C19 inhibitor	No	No	No
	CYP2C9 inhibitor	No	No	No
	CYP2D6 inhibitor	No	No	No
	CYP3A4 inhibitor	No	No	No
Excretion	Total clearance (log ml/min/kg)	0.237	0.263	0.496
	Renal OCT2 substrate	No	No	No
Toxicity	AMES toxicity	No	No	**Yes**
	Max. tolerated dose (human) (log mg/kg/day)	0.497	1.015	1.249
	hERG I inhibitor	No	No	No
	hERG II inhibitor	No	No	No
	Oral Rat Acute Toxicity (LD_{50}) (mol/kg)	2.503	2.303	2.084
	Hepatotoxicity	**Yes**	**Yes**	No
	Skin Sensitization	No	**Yes**	No
	Minnow toxicity (log mM)	2.712	0.619	2.872

compounds are neither P-glycoprotein substrates nor P-glycoprotein inhibitors.

The drug distribution is mainly analyzed based on human volume of distribution, human fraction unbound in plasma, blood-brain barrier, and central nervous system permeability. The steady-state volume of distribution (VDss) is a crucial pharmacokinetic parameter informing drug dose range design, representing the theoretical volume in which a drug dose would achieve similar blood plasma concentrations [47]. Higher VDss values indicate greater tissue distribution over plasma, with antibiotics and antivirals typically aiming for extensive tissue spread. VDss is deemed low if log (VDss) < -0.15, and high if log (VDss) > 0.45 [47]. In the present investigation, it was seen that the distribution of GMG-ITC and ibuprofen is lower. Similarly, the achieved results indicated a high fraction of unbound value to human plasma for all tested compounds which ranged between 0.239 and 0.813.

The Cytochrome P450 (CYP) enzyme group consists of isozymes responsible for metabolizing drugs, fatty acids, steroids, bile acids, and carcinogens. Drugs metabolism is dependent on their being a Cytochrome P450 substrate or inhibitor. The present study demonstrated that GMG-ITC and all investigated reference drugs did not act as a substrate or inhibitor of CYP enzymes (Table 2).

Excretion was analyzed through total clearance to determine whether or not GMG-ITC acts as a substrate of renal Organic cation transporter 2 (OCT2). The results indicated that none of the tested compounds were substrates of renal OCT2, suggesting they may be eliminated through an alternative route. Additionally, all the tested compounds exhibited a total clearance below log (CLtot) 1.0 mL/min/kg (Table 2), indicating high excretion clearance efficacy.

Toxicity analysis encompassed AMES results, maximum tolerated dose for humans, oral rat-acute toxicity, hepatotoxicity, skin sensitization, minnow toxicity, and determination of whether compounds act as inhibitors of the human ether-a-go-go-related gene (hERG). The results indicated that all tested compounds, except for 2-oxazolidinone, are non-mutagenic and non-carcinogenic. Furthermore, it was seen that GMG-ITC exhibited lower toxicity to humans compared to the tested reference drugs. The Maximum Recommended Tolerance Dose (MRTD) offers an estimation of the toxic dose in humans. According to Saha et al. (2021) [46], MRTD equal to or below log 0.477 (mg/kg/day) is classified as low. All tested compounds were found to be non-inhibitors of hERG, suggesting they do not block the K^+ channel. However, GMG-ITC and ibuprofen showed hepatotoxicity, while ibuprofen showed skin sensitivity. All the tested compounds showed high oral acute toxicity value (LD_{50}) (Table 2). A molecule with a higher oral rat acute toxicity (LD_{50}) value is less lethal compared to one with a lower LD_{50} value [46,47]. The lethal concentration values (LC_{50}) denote the concentration of a molecule required to induce 50 % fathead minnow mortality. A molecule is considered to have high acute toxicity if its log LC_{50} is less than 0.5 mM (log $LC_{50} < -0.3$) [46,47]. GMG-ITC, along with reference drugs, are less toxic as they exhibited good scores that are much higher than the above-mentioned LC_{50}.

3.4. Lipinski's rule of five, bioactivity score, and drug-likeness

Lipinski's rules of five (Ro5), bioactivity, and molecular properties were predicted by utilizing SwissADME, Molinspiration, and MolSoft software, respectively, and their results were summarized in Tables 3 and 4. Lipinski's rule of five expresses crucial molecular properties that influence a drug's pharmacokinetics within the human body, encompassing aspects such as absorption, distribution, metabolism, and elimination (ADME) [46]. The drug-likeness properties of the chosen compounds were assessed using Lipinski parameters. The obtained results indicate that none of the evaluated compounds violated Lipinski parameters (Table 3). Topological polar surface area (TPSA) calculation is indicative of the drug molecule's bioavailability and is closely linked to the compound's hydrogen bonding potential. The TPSA of the compounds was noticed in a range between 20.23 and 129.67 Å, which is well below the range of 160 Å [48]. According to Martin (2005) [49], any compound with a bioavailability score of $\geq$0.55 is considered ideal and absorbed very well by the body. The obtained data indicated good bioavailability and absorption for all tested compounds (Table 3).

A molecule with a bioactivity score above 0.00 is likely to exhibit significant biological activities; scores ranging from −0.50 to 0.00 are considered moderately active, while those below −0.50 are presumed to be inactive. Bioactivity scores of all compounds are illustrated in Table 4. It was demonstrated that GMG-ITC is highly active toward protease and enzyme inhibitors and moderately active toward GPCR ligand, ion channel modulator (ICM), nuclear receptor ligand (NRL), and kinase inhibitor (KI). Therefore, it is possible to state that GMG-ITC possesses higher biological activity than reference drugs.

3.5. Component-target analysis

To understand the multiple targets and various pathways in which GMG-ITC may interact in the human body, a component-target analysis was performed using Swiss Target Prediction. The parameter of probability value was set as 0.1 or 10 %. Altogether, 28 targets were obtained for GMG-ITC (Table 5).

3.6. GO and KEGG enrichment analysis

Performing GO and KEGG enrichment analysis of target genes associated with GMG-ITC using bioinformatics and visualizing the results (Fig. 6) provides valuable insights into its molecular mechanisms and

Table 3
Drug likeness properties.

Compounds	Lipinski Ro5	Molecular Weight (g/mol)	H-bond acceptors	H-bond donors	cLogP	TPSA (Å^2)	Bioavailability score
GMG-ITC	Yes; 0 violation	353.39	7	2	2.03	129.67	0.55
Ibuprofen	Yes; 0 violation	206.28	2	1	3.01	37.3	0.85
2-Oxazolidinone	Yes; 0 violation	87.08	2	1	−0.04	38.33	0.55

Table 4
Prediction of bioactivity score of compounds.

Compounds	GPCR[a]	ICM[b]	KI[c]	NRL[d]	PI[e]	EI[f]
GMG-ITC	0.07	0.06	−0.4	−0.05	0	0.51
Ibuprofen	−0.17	−0.01	−0.72	0.05	−0.21	0.12
2-Oxazolidinone	−3.47	−3.26	−3.67	−3.78	−3.23	−3.4

[a] GPCR ligand.
[b] ICM-ion channel modulator.
[c] KI- kinase inhibitor.
[d] NRL-nuclear receptor ligand.
[e] PI- protease inhibitor.
[f] EI- enzyme inhibitor.

potential biological pathways. The GO enrichment analysis ensued a total of 18 entries, with *p*-values adjusted using the Benjamini–Hochberg procedure to account for multiple tests, adhering to a significance threshold of $p < 0.05$.

In the category of BPs, the target proteins were primarily associated with the collagen catabolic process, extracellular matrix disassembly, extracellular matrix organization, adenosine receptor signaling pathway, cellular response to UV-A, proteolysis, response to beta-amyloid, activation of adenylate cyclase activity, and endodermal cell differentiation. In the molecular function (MF) class, the target proteins were predominantly associated with endopeptidase activity, metalloendopeptidase activity, serine-type endopeptidase activity, peptidase activity, G-protein coupled adenosine receptor activity, aspartic-type endopeptidase inhibitor activity, and alpha-glucoside transmembrane transporter activity. In the cellular component (CC) class, the target proteins were categorized as extracellular matrix and extracellular exosomes.

In KEGG analysis, a total of 14 KEGG-enriched items were identified, with corrected *p* values (h-corrected) below 0.05 were considered. GMG-ITC-associated pathways encompassed diverse physiological processes, including immune signaling (e.g., IL-17, TNF), metabolic pathways (e.g., Lipid metabolism, Carbohydrate digestion), and disease pathways (e.g., Cancer, Hepatitis B, Influenza). In our investigation, we used the GO terms (the so-called GO enrichment score) and the KEGG pathways to predict the relevance of GMG-ITC as a therapeutic agent and its potential efficacy in some relevant biological mechanisms. However, further investigation of its efficacy against MDR-initiated changes was not conducted.

3.7. MD simulation and analysis

3.7.1. Comparative stability and integrity analysis of protein-drug complexes

Comparative stability analysis of protein-drug complexes has been evaluated in terms of RMSD, RMSF, SASA, and Rg to assess structural integrity. RMSD tracks backbone deviation under MD force field influence, RMSF indicates residual fluctuation, Rg measures protein compactness, and SASA reflects solvent behaviour. In the present investigation, three different conditions were analyzed: protein-only system (proteins with no drugs), protein with control drugs, and proteins with selected drugs over a 100 ns MD trajectory. The superimposition of GMG-ITC on the targeted proteins was shown in Fig. 7 to observe the time-dependent protein-drug interaction.

Table 5
Molecular targets of GMG-ITC predicted from SwissTargetPrediction.

Molecular targets	GENE ID	UniProt ID	Probability Percentage of the Predicted Targets
Sodium/glucose cotransporter 2	SLC5A2, SGLT2	P31639	10 %
Adenosine A2a receptor (by homology)	ADORA2A	P29274	10 %
Adenosine A3 receptor	ADORA3	P0DMS8	10 %
S-methyl-5-thioadenosine phosphorylase (by homology)	MTAP, MSAP	Q13126	10 %
Sodium/glucose cotransporter 1	SLC5A1, NAGT, SGLT1	P13866	10 %
Adenosylhomocysteinase	AHCY, SAHH	P23526	10 %
Adenosine A2b receptor	ADORA2B	P29275	10 %
78 kDa glucose-regulated protein	HSPA5	A0A7P0TAI0	10 %
Hypoxanthine-guanine phosphoribosyltransferase	HPRT1, HPRT	P00492	10 %
Glyceraldehyde-3-phosphate dehydrogenase liver	GAPDH, GAPD, CDABP0047, OK/SW-cl.12	P04406	10 %
Thymidylate synthase	TYMS, TS, OK/SW-cl.29	P04818	10 %
ADAM17	SORL1, C11orf32	Q92673	10 %
Matrix metalloproteinase 13	MMP13	P45452	10 %
Matrix metalloproteinase 1	MMP1	A5GZ69	10 %
Matrix metalloproteinase 7	MMP7	P09237	10 %
Phosphodiesterase 8 B	PDE8B	D6RJD7	10 %
Matrix metalloproteinase 8	MMP8, CLG1	P22894	10 %
P-glycoprotein 1	ABCB1	P08183	10 %
Caspase-3	CASP3, CPP32	P42574	10 %
Platelet-activating factor receptor (by homology)	PTAFR, PAFR	P25105	10 %
Sodium/nucleoside cotransporter 2	SLC28A2, CNT2	O43868	10 %
Heat shock cognate 71 kDa protein	HSPA8, HSC70, HSP73, HSPA10	P11142	10 %
Dual specificity mitogen-activated protein kinase kinase 1	MAP2K1, MEK1, PRKMK1	Q02750	10 %
Hexokinase type II	HK2	P52789	10 %
Interleukin-1 receptor-associated kinase 4	IRAK4	Q9NWZ3	10 %
Matrix metalloproteinase 3	MMP3	P08254	10 %
Matrix metalloproteinase 9	MMP9, CLG4B	P14780	10 %
Transmembrane domain-containing protein TMIGD3	TMIGD3, UNQ1931/PRO4406	P0DMS9	10 %

3.7.2. RMSD analysis

RMSD analysis reveals that protein-only systems and their docked ligand complexes exhibit distinct backbone stability profiles due to solvation effects and environmental conditions (Fig. 8). Hydrophobic surfaces are destabilized in aqueous environments by TIP3P molecules, causing increased RMSD fluctuations and altered protein folding, while hydrophilic surfaces remain stable through interactions with TIP3P water. This highlights the role of solvation effects in protein stability and dynamics. Modified protein structures showed average RMS deviations of approximately ~0.27–0.93 nm. Protein-control drug complexes exhibited deviations ranging from ~0.15 to 1.14 nm, while proteins-

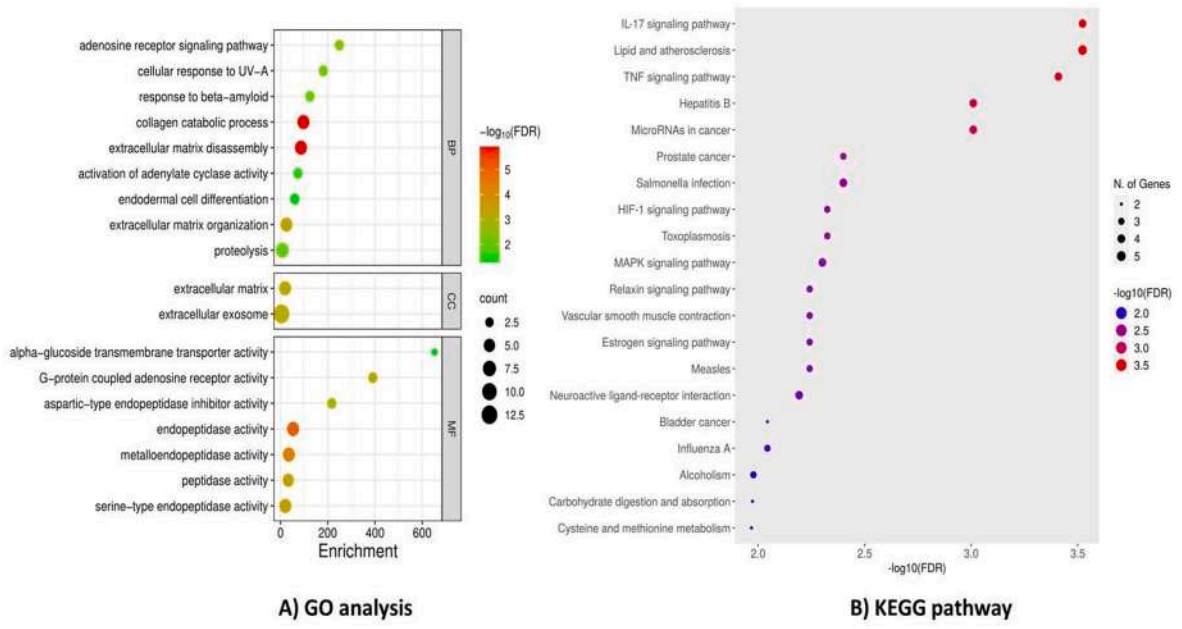

Fig. 6. GO and KEGG analysis results for GMG-ITC.

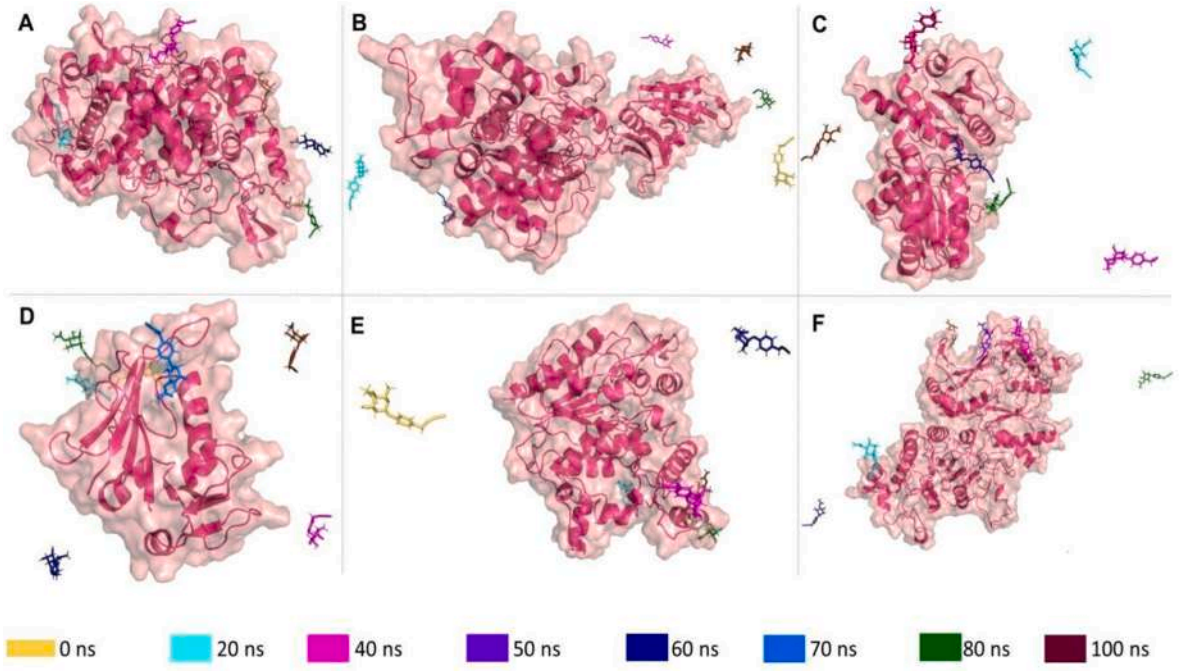

Fig. 7. Superimposition of selected drug molecule (GMG-ITC) on the targeted (A)1CX2, (B)1MWU (C) 3N8D (D) 3SRW (E) 6KSI (F) 3J25 at the time interval of 10/20 ns (ns) to observe the time-dependent protein-drug interaction. The trajectory of the same drug molecules in different time frames is depicted in specific color codes.

GMG-ITC complexes displayed deviations ranging from ~0.15 to 0.98 nm, indicating varying degrees of structural perturbation induced by different ligands. Fig. 8 demonstrates that the docked ligand complexes of 1CX2 (panel A), 6KSI (panel E), and 3J25 (panel F) exhibit substantial backbone deviations during the intervals of 15–100 ns, 2–62 ns, and 20–100 ns, respectively, compared to their protein-only systems counterparts. This suggests that ligand binding prompts the remodelling of protein conformation and accelerates protein folding dynamics. Additionally, the observed backbone instability of the 1CX2, 6KSI, and 3J25 protein-only systems from the beginning of the MD simulation underscores the hydrophobic nature of the protein surfaces and the consequent desolvation effects. Ligand interactions alleviate reduced solvation effects, causing unsteady RMSD routes for the 1CX2, 6KSI, and 3J25 protein-ligand complexes. Notably, 3J25 shows greater deviations with 2-Oxazolidinone than with GMG-ITC, indicating enhanced backbone stability and interaction with GMG-ITC, as validated by hydrophobic interaction energy decomposition (Fig. 13). Similarly, the 1CX2-ibuprofen complex shows more erratic deviations compared to interactions with GMG-ITC, indicating greater stability with GMG-ITC, supported by energy decomposition as well (Fig. 13). In contrast, the stabilized backbone dynamics and protein folding landscape of 6KSI-GMG-ITC compared to 6KSI-2-Oxazolidinone suggest more consistent

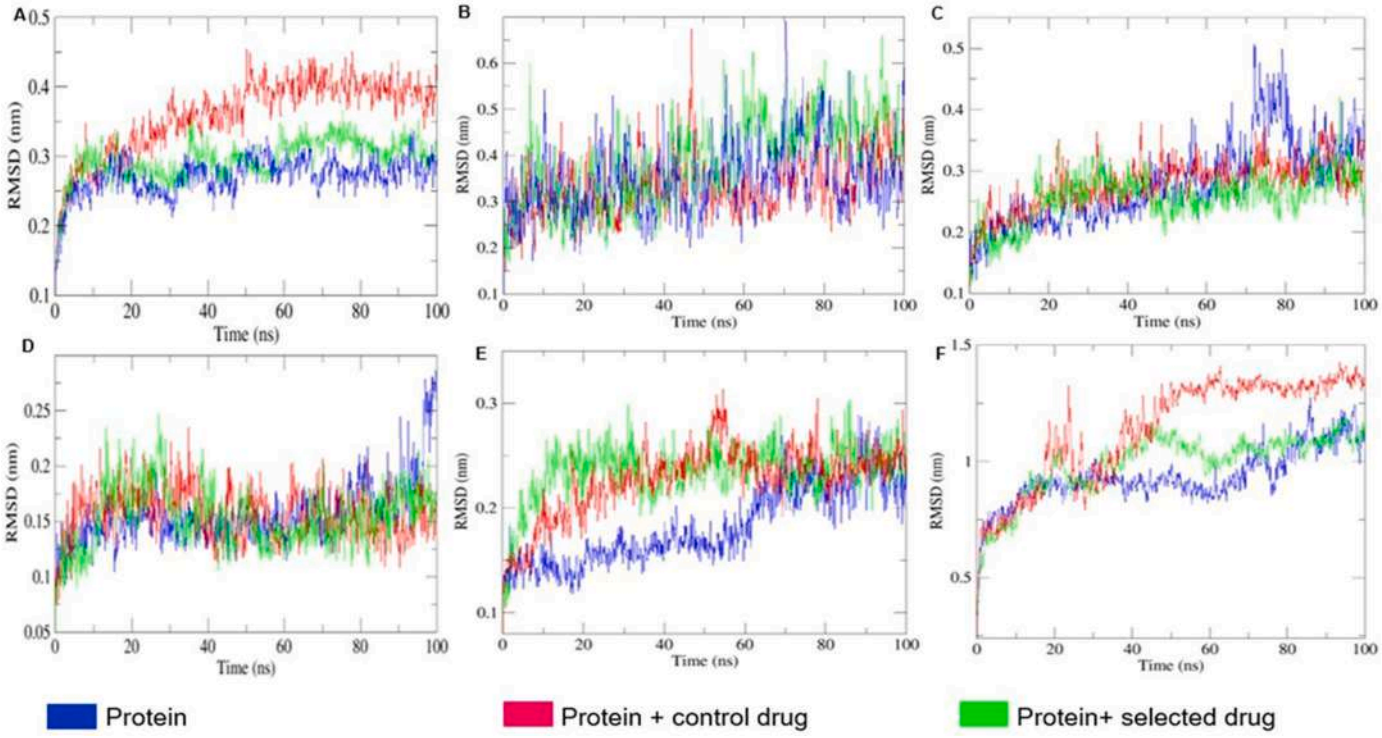

Fig. 8. Comparative analyses of RMSD of three different backbones of proteins (protein only, proteins with control drug, and proteins with selected drug) throughout 100 ns of MD run. (A)1CX2, (B)1MWU (C) 3N8D (D) 3SRW (E) 6KSI (F) 3J25. For subfigure A the control drug is Ibuprofen and for panel B, C, D, E, and F the control drug is 2-Oxazolidinone.

electrostatic interactions, supported by hydrogen bond formation (Fig. 12).

3.7.3. *RMSF analysis*

RMSF analyses revealed increased flexibility of Cα backbone and amino acid residues in proteins when paired with selective docked ligands over the 100 ns MD interval, compared to fluctuations observed in respective protein-only systems. In Fig. 9, panels A, B, C, D, E, and F displayed RMSF values ranging approximately as 0.17 ± 0.01 nm, 0.26 ± 0.15 nm, 0.21 ± 0.02 nm, 0.13 ± 0.12 nm, 0.13 ± 0.14 nm, and 0.32 ± 0.16 nm. Despite similar average fluctuation values between protein-only systems and protein-docked ligand complexes, noticeable abrupt

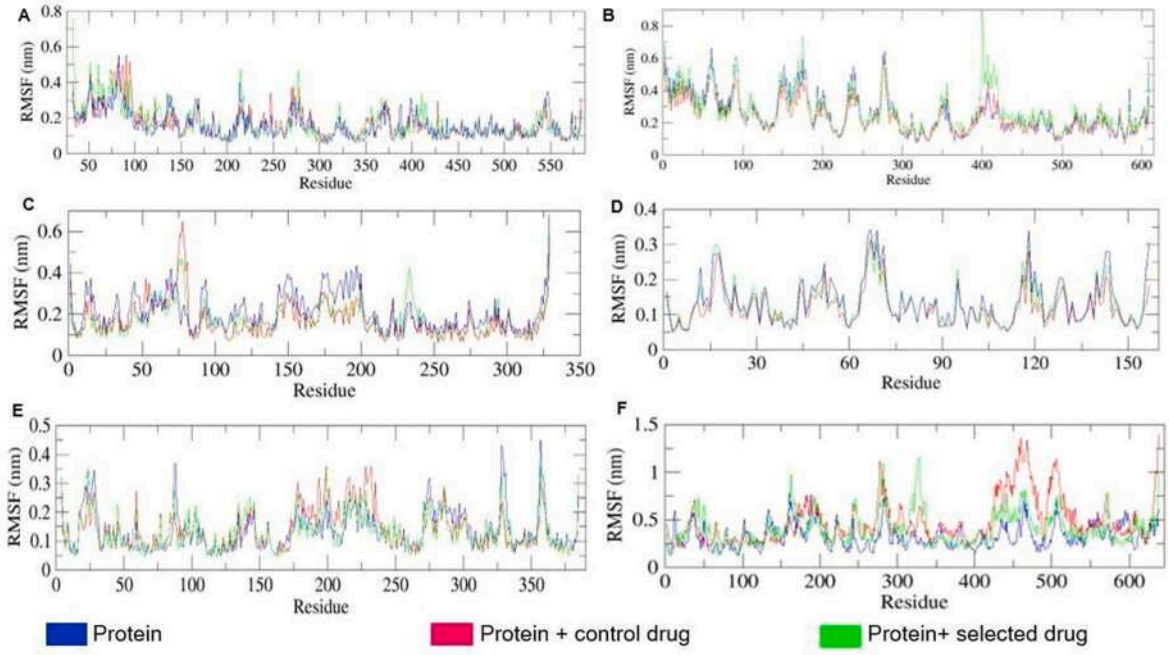

Fig. 9. Comparative analysis of RMSF of consecutive amino acids present in different proteins under the effect of no drugs, control drug, and selected drug specific for those proteins in the dynamic environment MD simulation. The proteins, control drugs, and selected drugs depicted in the subfigures are the same in correspondence to the respective panels A, B, C, D, E, and F of Fig. 7.

fluctuations in the latter during intermediate intervals of the MD trajectory suggest significant interactions between amino acid residues and ligand molecules. Similarly, increased fluctuations were observed at the 75th residue (3N8D-docked complexes), 400th residue (1MWU-GMG-ITC), 195th and 225th residues (6KSI-2-Oxazolidinone), 330th residue (3J25-GMG-ITC), and 450th and 500th residues (3J25-ligand docked complexes), indicating higher flexibilities in interaction with specific ligand molecules.

3.7.4. SASA and R_g analysis

SASA plots (Fig. 10) were analyzed to interpret the solvent behaviour of proteins in three selective environments (protein-only system, proteins with control drugs, and selected drugs). Additionally, SASA revealed hydrophobic interactions of proteins in the presence of docked ligands. SASA values for protein combinations 1CX2, 1MWU, 3N8D, 3SRW, 6KSI, and 3J25 ranged between 240 and 280 nm^2, 300–340 nm^2, 160–190 nm^2, 87–102 nm^2, 170–195 nm^2 and 330–410 nm^2 respectively. These plots indicated significant hydrophobic occupation between proteins and docked complexes.

The compactness and structural integrity of protein-docked ligand conformations were assessed through R_g fluctuations (Fig. 11). The average R_g values for different protein combinations (proteins and protein-docked ligand complexes) 1CX2, 1MWU, 3N8D, 3SRW, 6KSI, and 3J25 were 2.49 ± 0.04 nm, 3.69 ± 0.2 nm, 2.24 ± 0.15 nm, 1.57 ± 0.04 nm, 2.09 ± 0.07 nm, and 3.05 ± 0.55 nm, respectively. Notably, in panels E and F, the average R_g of protein-docked ligand complexes throughout the MD trajectory was more prominent than the respective proteins, indicating a gradual deterioration of compactness in the presence of docked ligands during increased MD intervals. However, comparative studies revealed that the degree of compactness and stability of protein-selected drug complexes were better than that of protein-reference drug complexes, as the average R_g fluctuations of protein-selected drug complexes maintained closer alignment with R_g fluctuations of respective protein-only systems throughout the entire 100 ns MD interval.

3.7.5. Analysis of H bonds based subsequent pairing analysis

Hydrogen bonds (H bonds) act as the decisive "master key to molecular recognition," crucial for ligand-dependent enzyme catalysis. The binding affinity of docked ligands with specific proteins was assessed based on the H bond formation of ligands-proteins interaction (Fig. 12). In the case of 1CX2–GMG-ITC, two hydrogen bonds were detected, thus corroborating the molecular docking result. For the 1MWU–GMG-ITC complex, only one hydrogen bond was initially detected, however, over time, it was increased and three H bonds were detected at the end. For the complex 3N8D–GMG-ITC, two H bonds were found in the initial point, but at the end, three H bonds were detected. For 3SRW–GMG-ITC, two H-bonds were detected at the starting point, then their number increased to three H bonds, and finally, their number reduced to two H bonds which was very close to docking interaction analysis. The protein-ligand complex 6KSI–GMG-ITC showed only one H bond initially, which increased to two H bonds and, at the endpoint it was detected two H bonds. In the complex 3J25–GMG-ITC, three H bonds throughout a particular MD interval have been detected. All detected H bonds of all protein-ligand complexes showed a similarity with docking results. Comparison with control drug-protein complexes (Fig. 12B) revealed less occupancy, suggesting more persistent and stable binding affinities of selected drugs over reference drugs throughout the 100 ns MD trajectory. These simulation studies further support and validate the 2D docking interaction studies.

3.7.6. Analysis of interaction energy

Interaction energy was analyzed in terms of short-range electrostatic (Coul-SR) and van der Waals/hydrophobic (LJ-SR) interactions. Average values of Coul-SR energy (in KJ/mol) for protein-selected drugs (Fig. 13A) and protein-control drugs (Fig. 13B) ranged as follows: 2.58 × 10^6 kJ/mol (1CX2–GMG-ITC), −8.62 × 10^6 kJ/mol (1MWU–GMG-ITC), −1.97 × 10^6 kJ/mol (3N8D–GMG-ITC), −1.07 × 10^6 kJ/mol (3SRW–GMG-ITC), −1.98 × 10^6 kJ/mol (6KSI–GMG-ITC), and −6.03 × 10^6 kJ/mol (3J25–GMG-ITC). For protein-control drugs, the values were: 2.58 × 10^6 kJ/mol (1CX2–ibuprofen), −8.62 × 10^6 kJ/mol

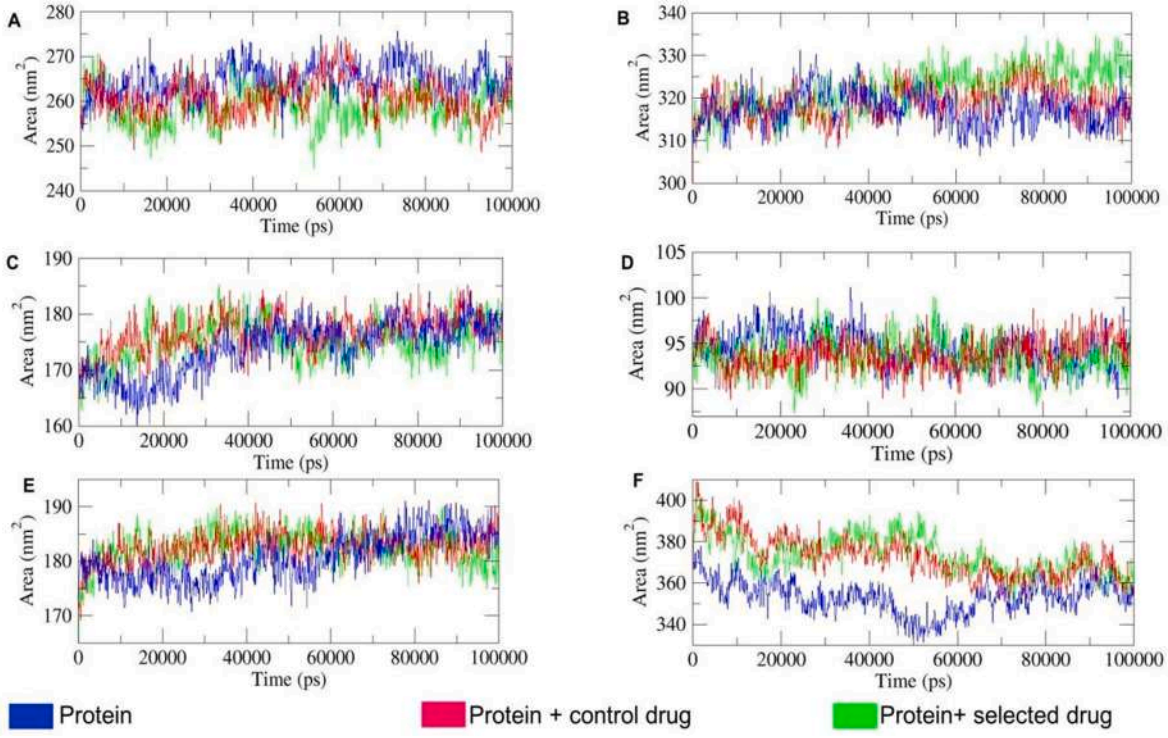

Fig. 10. SASA analysis of proteins in 3 different environments is represented in this figure designated by different color codes. The proteins, control drugs and selected drug used in the specific subfigures are respectively same as depicted in the explicit panels A, B, C, D, E, and F in Fig. 7.

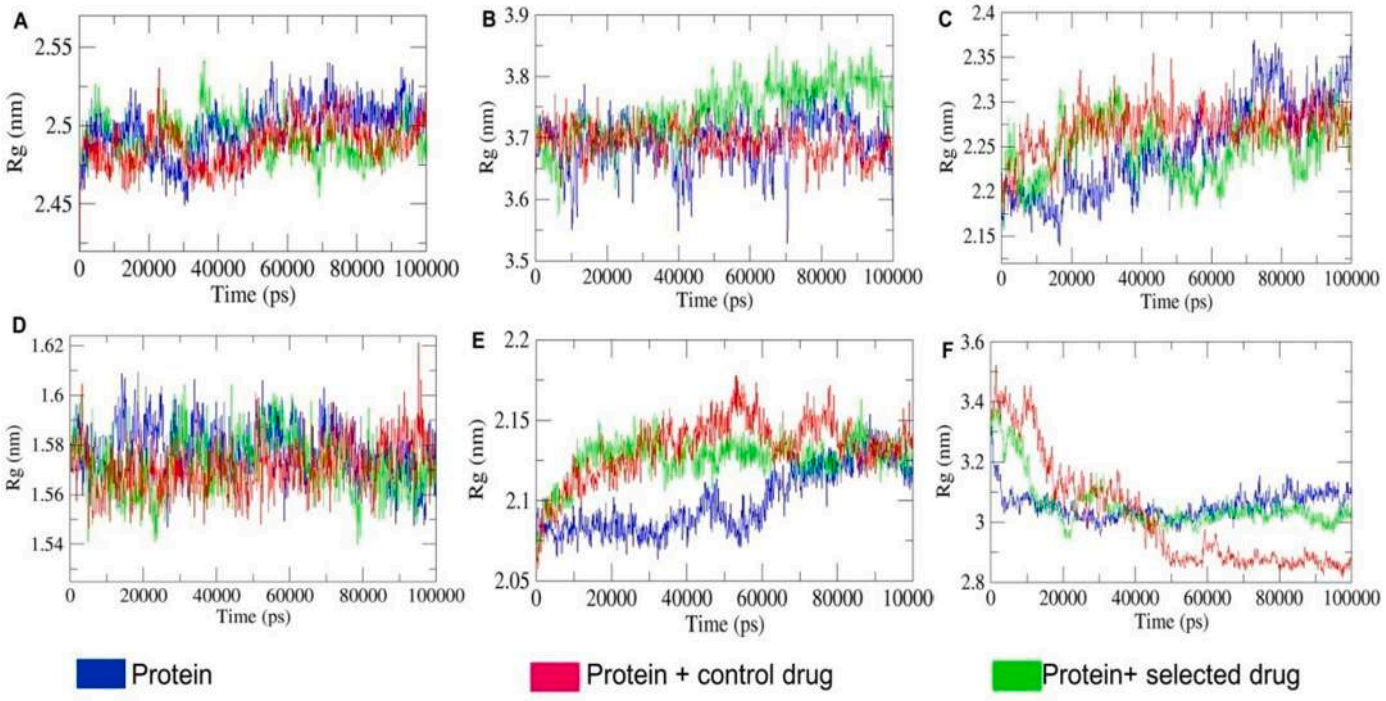

Fig. 11. R_g of proteins in 3 MD environments (without drugs, with control drugs, with selected drug) are reported where the proteins, control drugs, and selected drug in specific subfigures are respectively same as mentioned in the corresponding panels A, B, C, D, E, and F of Fig. 7.

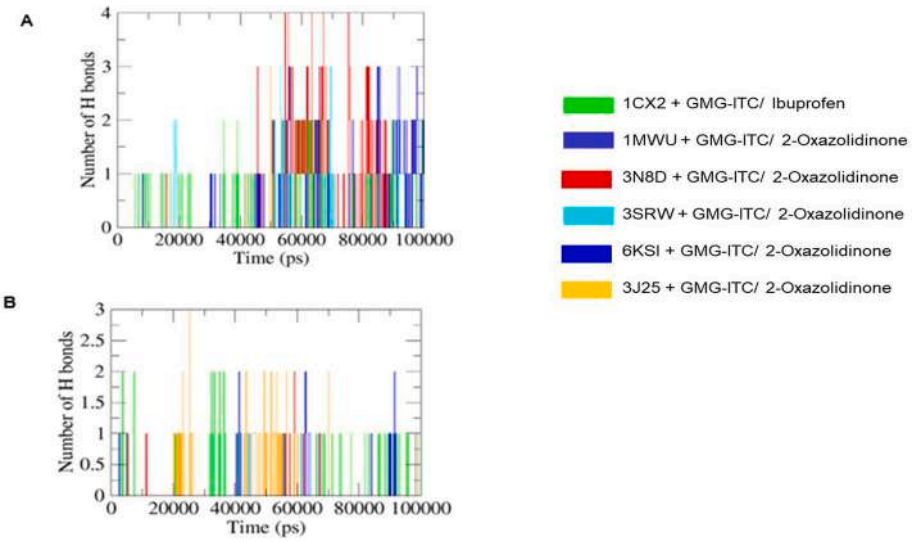

Fig. 12. Figure illustrates the total number of hydrogen (H) bonds formation and pairing (within 0.35 nm) of proteins to selected drug (GMG-ITC) and control drugs (ibuprofen and 2-Oxazolidinone to specific proteins) up to 100,000 ps (ps) depicted respectively in subfigure A and B.

(1MWU–2-Oxazolidinone), −2.58 × 10^6 kJ/mol (3N8D–2-Oxazolidinone), −1.07 × 10^6 kJ/mol (3SRW–2-Oxazolidinone), −1.98 × 10^6 kJ/mol (6KSI–2-Oxazolidinone), and −6.03 × 10^6 kJ/mol (3J25–2-Oxazolidinone). Similarly, the interpreted data of LJ-SR energy showed the dynamics of selected drug-protein (Fig. 13C) and control drug-protein (Fig. 13D). The average LJ-SR energy ranged as follows: 2.1 × 10^5 kJ/mol (1CX2–GMG-ITC), 7.68 × 10^5 kJ/mol (1MWU–GMG-ITC), 1.62 × 10^5 kJ/mol (3N8D–GMG-ITC), 0.9 × 10^5 kJ/mol (3SRW-GMG-ITC), 1.62 × 10^5 kJ/mol (6KSI–GMG-ITC), and 5.25 × 10^5 kJ/mol (3J25-GMG-ITC). For control drug-protein dynamics, the values were: 2.07 × 10^5 kJ/mol (1CX2–ibuprofen), 7.65 × 10^5 kJ/mol (1MWU–2-Oxazolidinone), 2.2 × 10^5 kJ/mol (3N8D–2-Oxazolidinone), 0.9 × 10^5 kJ/mol (3SRW–2-Oxazolidinone), 1.62 × 10^5 kJ/mol (6KSI–2-Oxazolidinone), and 5.25 × 10^5 kJ/mol (3J25–2-Oxazolidinone). The steady energy flow of protein-docked ligand complexes throughout the whole MD trajectory backed docking results and stability of the complexes and, more precisely, signifies that hydrophobic/van der Waals, as well as electrostatic interaction, have played a crucial role in consistent equilibration of the protein-ligand interactions in a diverse set of ion-solvent MD environment.

4. Discussion

In the present study, GMG-ITC was screened against potential

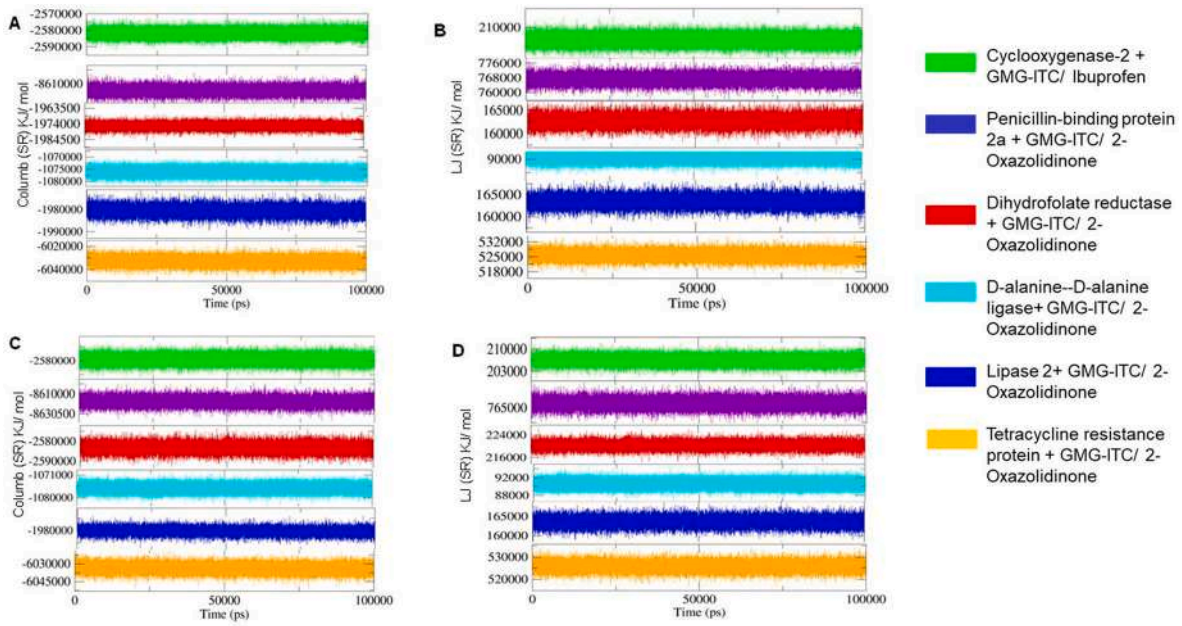

Fig. 13. Coulomb (SR) energy is represented by panels A and C based on the MD interaction of proteins with selected drug (GMG-ITC) and control drug (ibuprofen/2-Oxazolidinone) respectively. Similarly, LJ (SR) energy is illustrated by panels B and D based on the same interaction study. Comparative analyses of different combinations are displayed with the above-mentioned color codes.

molecular drug targets of MDR *S. aureus* and its anti-inflammatory and antioxidant potential was also analyzed. It is well-established that natural products have long been key sources for pharmaceutical discoveries, with many plant-derived compounds such as flavonoids, alkaloids, phenols, lactones, and terpenes showing promising antibacterial properties [17,35].

M. oleifera, renowned in traditional medicine, offers diverse pharmacological advantages attributed to its rich phytochemical profile. Particularly noteworthy is GMG-ITC, a potent compound found in its seeds, which is released through the hydrolysis of GMG by the myrosinase enzyme. GMG-ITC has a history in drug development, underscoring its potential therapeutic significance. Previous research highlights its broad pharmacological properties, including antimicrobial, anti-inflammatory, antioxidant, antidiabetic, anticancer, antiulcer, and neuroprotective activities [20,22,50], with notable antibacterial effects against *S. aureus* and its multidrug-resistant variants [23,51].

In this study, GMG-ITC showed the best binding affinity toward *S. aureus* lipase (SAL) with a docking score of −7.1 kcal/mol. *S. aureus* lipase is triacylglycerol esterase, which is an important virulence factor responsible for its pathogenesis, mainly degrades the immune-responsive lipids and inhibits the activation of innate immune cells, and also interferes with the host immune system to affect innate immune recognition in the microbe [25]. Therefore, SAL is one of the drug targets for inhibiting *S. aureus* infections. However, very few SAL inhibitors have been introduced to date, so the binding affinity of GMG-ITC with SAL demonstrates its potential as a probable SAL inhibitor for further drug development interventions. Similarly, GMG-ITC exhibited strong binding affinity with dihydrofolate reductase (−7.8 kcal/mol), which is essential for bacterial survival as dihydrofolate reductase is involved in the thymidine synthesis pathway that is essential for DNA synthesis. So, the inhibition of dihydrofolate reductase can inhibit the further replication of microbes. For MRSA, penicillin-binding protein **2a** (1MWU) is a probable drug target for combating MDR bacteria, which possess cell wall biosynthesis in the presence of β-lactams [52]. Similarly, D-Ala: D-Ala ligase (3N8D), MepR transcription regulator (3ECO), and RPP TetM in complex with the 70 S ribosome (3J25) are the molecular targets to address the threat of other MDR variants of *S. aureus* such as VRSA-9, TRSA, TetRSA, respectively [28,30,31]. GMG-ITC exhibited a good docking score with all of these protein targets compared to the studied reference drug 2-Oxazolidinone (Table 1) representing it as a potential candidate for inhibition of MDR *S. aureus*. Further, antioxidant and anti-inflammatory activity was evaluated to check its potentiality to minimize oxidative stress and to reduce inflammation in the human cells procured due to bacterial infection. GMG-ITC showed the best binding affinity with cyclooxygenase-2 (−7.5 kcal/mol) which catalyzes the biosynthesis of pro-inflammatory prostanoids. COX inhibitors are commonly employed to alleviate both acute and chronic pain as well as inflammation [53]. These results demonstrate the potentiality of GMG-ITC to reduce bacterial inflammation in the body. Galuppo et al. (2014) [54] reported the anti-inflammatory activity of GMG-ITC in a mouse model against autoimmune encephalomyelitis. Another study by Jaafaru et al. (2018) [55] also reported that GMG-ITC induces apoptosis and inhibits proliferation of human prostate adenocarcinoma cells. Similarly, GMG-ITC showed a well-binding interaction with FAD-dependent NAD(P)H oxidase, which is primarily involved in ROS production [56]. Therefore, a strong inhibition of this enzyme by GMG-ITC can minimize cellular oxidative stress. A study by Tumer et al. (2015) [57] showed the direct and indirect antioxidant activity of GMG-ITC.

Depending on the docking analysis, further pharmacokinetic study was performed to analyze GMG-ITC as a potent drug. In the present investigation, it was demonstrated that GMG-ITC has moderate solubility and permeability with a high absorption rate in the human intestine indicating its high bioavailability and low variability [58]. Additionally, GMG-ITC showed a high fraction of unbound value in human plasma, indicating a substantial amount of free fraction available for interaction with targeted proteins. This suggests enhanced potential for drug activity. Also, GMG-ITC showed an excretion clearance efficiency along with less toxicity. Further, the studied candidate is not mutagen or carcinogen and is less lethal with high oral acute toxicity, indicating that it is a potential drug candidate. Any potential drug typically binds with a biological target, often enzymes, ion channels, and receptors. GMG-ITC exhibits high activity toward protease and enzyme inhibitors while showing moderate activity toward GPCR ligands, ICM, NRL, and KI.

Enrichment analysis highlights GMG-ITC's involvement in various

biological processes, including tissue remodelling, repair, and homeostasis. It affects processes like collagen breakdown, extracellular matrix disassembly, and endodermal cell organization [59,60]. Additionally, GMG-ITC can influence cellular responses through adenosine receptor signaling and adenylate cyclase activation [61]. It also exhibited a promising approach to protect against UV-induced damage and neuroprotection from beta-amyloid toxicity [62]. Its impact on proteolytic processes suggests a role as a protease inhibitor or modulator, aligning with the biological activity findings in this investigation. Furthermore, GMG-ITC is implicated in diverse enzymatic functions like endopeptidase, metalloendopeptidase, and serine-type endopeptidase activity, hinting at its role in regulating proteolytic processes [59]. It may also hinder aspartic-type endopeptidases. Additionally, GMG-ITC is associated with G-protein coupled adenosine receptor and Alpha-glucoside transmembrane transporter activities, possibly impacting adenosine receptor signaling and glucose transport regulation. Its presence in the extracellular matrix and exosomes suggests cell-cell communication and signaling involvement. KEGG analysis links GMG-ITC to immune signalling pathways such as IL-17, and TNF, suggesting a role in immune response modulation [63,64]. It also indicates GMG-ITC's involvement in metabolic pathways (e.g., lipid metabolism, carbohydrate digestion) and potential therapeutic applications in diseases like cancer, hepatitis B, and influenza.

MD simulation showed the interaction of the GMG-ITC with selected proteins and its outputs. RMSD values remained stable for all interactions except 1CX2, 6KSI, and 3J25. However, interactions of GMG-ITC demonstrate greater stability compared to protein-control drug interactions. RMSD plots illustrate the influence of SASA on hydrophobic and hydrophilic protein surfaces, ligand-induced protein folding alterations, and solvation dynamics via backbone fluctuations. H-bond analysis reveals that GMG-ITC forms more favorable electrostatic interactions than 2-Oxazolidinone and ibuprofen with proteins 1CX2, 1MWU, 3N8D, 3SRW, and 6KSI, evidenced by higher H-bond intensity. This consistency with docking scores substantiates the docking performance. Due to the volumetric size of proteins, particularly in the 3J25 system, there is an extensive hydrophobic surface area, resulting in decreased compactness and accelerated protein folding. This is evidenced by pronounced hydrophobic interactions upon 3J25-docked complex formation. Specifically, the interaction between 3J25 and GMG-ITC results in greater hydrophobic energy dissipation than the 3J25 and 2-Oxazolidinone interaction, as supported by SASA (Fig. 10) and energy decomposition plots (Fig. 13). Notable integrity in the Rg trajectory, overlapping RMSD routes, and residual fluctuations in the RMSF plot highlight solvation and desolvation effects in ligand interactions and protein folding stability, especially in 3N8D, as validated by increased H-bond formation (Fig. 12). The Rg value of proteins and protein-ligand complex indicate the compactness and integrity of proteins in the presence of GMG-ITC compared to control drugs. Ligand-induced backbone instability, residual flexibility, and accelerated folding are notable in 1CX2, 6KSI, and 3J25 complexes, unlike the more stable 3SRW and 1MWU. The 1MWU and 3SRW systems exhibit heightened solvation effects and minimal electrostatic interactions, with fewer H bonds and reduced electrostatic energy dissipation. The MD simulations collectively reinforce the docking findings, confirming the stability of the complex formed by the interaction of six different proteins with GMG-ITC compared to selected control drugs, characterized by high structural compactness and minimal to no fluctuations.

These findings indicate that GMG-ITC can be a potential antibacterial drug against *S. aureus* infections and also can be able to reduce infection-related inflammation and oxidative stress. However, Phytochemical-based drug discovery via molecular docking and ADMET analysis offers a robust, efficient, and cost-effective method for identifying novel antibacterial agents. This approach enables rapid screening of natural compounds with high throughput and detailed molecular interaction insights, addressing multi-drug resistance without extensive lab work. Similarly, Mallick et al. (2022, 2023) demonstrated the potential of docking and ADMET analysis for novel therapeutic development [65,66]. Nevertheless, *in silico* methods depend on structural data, which may not fully predict actual pharmacokinetics, toxicity, protein dynamics, cellular environment, and off-target effects. To enhance prediction accuracy, deep learning methods and high-throughput computational models, such as a multistep Laplace-optimized decomposition method and an optimized hybrid approach using a KNN classifier, could be acquired and planned for future studies [67–69]. Additionally, *in vitro* and *in vivo* studies will be performed to validate the predicted activity and confirm the antimicrobial efficacy of GMG-ITC against MDR *S. aureus* strains.

5. Conclusion

This study evaluated the antibacterial potential of GMG-ITC against MDR *S. aureus* through *in silico* docking approach, revealing inhibitory efficacy and promising molecular interactions with key bacterial proteins. Also, GMG-ITC demonstrated favorable docking scores with anti-inflammatory and antioxidant proteins, indicating its potential to mitigate infection-induced inflammation and cellular damage. Further, MD simulations support docking results, confirming the stability of the GMG-ITC complex with targeted proteins. GO enrichment analysis underscored its efficacy in tissue remodelling, repair, maintaining homeostasis, regulating proteolytic processes, glucose transport, and intercellular communication. Additionally, KEGG analysis suggested its potential therapeutic applications in diseases such as cancer, hepatitis B, and influenza. Moreover, a comprehensive pharmacokinetic and bioactivity profile supports GMG-ITC as a promising candidate for drug development. This systematic analysis bridges *in vitro* and *in vivo* antibacterial activities, providing insights into the molecular mechanisms and paving the way for further investigations into *S. aureus* infection prevention. Furthermore, this study hints at GMG-ITC's potential to counteract MDR *S. aureus* pathogenesis. Nevertheless, rigorous *in vitro* and *in vivo* pharmacological evaluation and quality assessment are imperative to validate its practical applicability.

Funding

Project SPIA—Valorization of by-products from the agro-food chain CUP: G49J19001350004; and DGR n. 527/2019 "PO FESR BASILICATA 2014–2020—Axis I—Research, Innovation Action and Technological Development—Action 1 B.1.2.1—Avviso Pubblico per il sostegno alla creazione e sviluppo dei Cluster Tecnologici della Regione Basilicata e alla realizzazione di progetti di Ricerca e Sviluppo"; Project NODES, which has received funding from the MUR – M4C2 1.5 of PNRR funded by the European Union - NextGenerationEU (Grant agreement no. ECS00000036 – CUP B43D21010950006).

CRediT authorship contribution statement

Soham Bhattacharya: Writing – review & editing, Writing – original draft, Visualization, Methodology, Formal analysis, Data curation, Conceptualization. **Adrish Dutta:** Writing – review & editing, Visualization, Methodology, Formal analysis. **Pijush Kanti Khanra:** Writing – review & editing, Visualization, Methodology, Formal analysis. **Neha Gupta:** Writing – review & editing, Validation, Formal analysis. **Ritesh Dutta:** Writing – review & editing, Visualization, Formal analysis. **Nikolay T. Tzvetkov:** Writing – review & editing, Supervision, Formal analysis. **Luigi Milella:** Writing – review & editing, Funding acquisition, Formal analysis. **Maria Ponticelli:** Writing – review & editing, Supervision, Formal analysis.

Declaration of competing interest

The authors declare that they have no known competing financial interests or personal relationships that could have appeared to influence

the work reported in this paper.

Acknowledgements

The authors also acknowledged Prof. Eloy Fernandez-Cusimamani (Faculty of Tropical AgriSciences, Czech University of Life Sciences in Prague) for consultation and technical assistance.

Appendix A. Supplementary data

Supplementary data to this article can be found online at https://doi.org/10.1016/j.compbiomed.2024.108907.

References

[1] Antimicrobial Resistance, 2023. https://www.who.int/news-room/fact-sheets/detail/antimicrobial-resistance. (Accessed 20 February 2024).
[2] C.J.L. Murray, K.S. Ikuta, F. Sharara, L. Swetschinski, G. Robles Aguilar, A. Gray, C. Han, C. Bisignano, P. Rao, E. Wool, S.C. Johnson, A.J. Browne, M.G. Chipeta, M. Naghavi, Global burden of bacterial antimicrobial resistance in 2019: a systematic analysis, Lancet 399 (2022) 629–655, https://doi.org/10.1016/S0140-6736(21)02724-0.
[3] Drug-Resistant Infections, A Threat to Our Economic Future, World Bank, 2016. https://www.worldbank.org/en/topic/health/publication/drug-resistant-infections-a-threat-to-our-economic-future. (Accessed 20 February 2024).
[4] A.N. Poudel, S. Zhu, N. Cooper, P. Little, C. Tarrant, M. Hickman, G. Yao, The economic burden of antibiotic resistance: a systematic review and meta-analysis, PLoS One 18 (2023) e0285170, https://doi.org/10.1371/journal.pone.0285170.
[5] R.H. Drew, Emerging options for treatment of invasive, multidrug-resistant *Staphylococcus aureus* infections, Pharmacotherapy 27 (2007) 227–249, https://doi.org/10.1592/phco.27.2.227.
[6] S. Gatadi, Y.V. Madhavi, S. Chopra, S. Nanduri, Promising antibacterial agents against multi-drug resistant *Staphylococcus aureus*, Bioorg. Chem. 92 (2019) 103252, https://doi.org/10.1016/j.bioorg.2019.103252.
[7] B. Mlynarczyk-Bonikowska, C. Kowalewski, A. Krolak-Ulinska, W. Marusza, Molecular mechanisms of drug resistance in *Staphylococcus aureus*, Int. J. Mol. Sci. 23 (2022) 8088, https://doi.org/10.3390/ijms23158088.
[8] M. Shoaib, A.I. Aqib, I. Muzammil, N. Majeed, Z.A. Bhutta, M.F.-A. Kulyar, M. Fatima, C.-N.F. Zaheer, A. Muneer, M. Murtaza, M. Kashif, F. Shafqat, W. Pu, MRSA compendium of epidemiology, transmission, pathophysiology, treatment, and prevention within one health framework, Front. Microbiol. 13 (2023) 1067284, https://doi.org/10.3389/fmicb.2022.1067284.
[9] M. Huemer, S. Mairpady Shambat, S.D. Brugger, A.S. Zinkernagel, Antibiotic resistance and persistence—implications for human health and treatment perspectives, EMBO Rep. 21 (2020) e51034, https://doi.org/10.15252/embr.202051034.
[10] C. Browne, N. Muszbek, R. Chapman, K. Marsh, I.M. Gould, R.A. Seaton, M. Allen, Comparative healthcare-associated costs of methicillin-resistant *Staphylococcus aureus* bacteraemia-infective endocarditis treated with either daptomycin or vancomycin, Int. J. Antimicrob. Agents 47 (2016) 357–361, https://doi.org/10.1016/j.ijantimicag.2016.02.006.
[11] P.O. Lewis, E.L. Heil, K.L. Covert, D.B. Cluck, Treatment strategies for persistent methicillin-resistant *Staphylococcus aureus* bacteraemia, J. Clin. Pharm. Therapeut. 43 (2018) 614–625, https://doi.org/10.1111/jcpt.12743.
[12] A. Bansal, C. Priyadarsini, A. Bansal, C. Priyadarsini, Medicinal properties of phytochemicals and their production, in: Natural Drugs from Plants, IntechOpen, 2021, https://doi.org/10.5772/intechopen.98888.
[13] M. Liang, X. Ge, H. Xua, K. Ma, W. Zhang, Y. Zan, T. Efferth, Z. Xue, X. Hua, Phytochemicals with activity against methicillin-resistant *Staphylococcus aureus*, Phytomedicine 100 (2022) 154073, https://doi.org/10.1016/j.phymed.2022.154073.
[14] T. Kebede, E. Gadisa, A. Tufa, Antimicrobial activities evaluation and phytochemical screening of some selected medicinal plants: a possible alternative in the treatment of multidrug-resistant microbes, PLoS One 16 (2021) e0249253, https://doi.org/10.1371/journal.pone.0249253.
[15] R.A. El-Shiekh, R. Elshimy, A.A. Mandour, H.A.H. Kassem, A.E. Khaleel, S. Alseekh, A.R. Fernie, M.A. Salem, Phytochemical characterisation of leaves and stems of *Murraya koenigii* (L.) Sprengel and *Murraya paniculata* (L.) Jack and their antibacterial activity against multidrug-resistant *Acinetobacter baumannii* bacterial infection, Int. J. Food Sci. Technol. (2024), https://doi.org/10.1111/ijfs.17032.
[16] E.P. Padla, L.T. Solis, R.M. Levida, C.-C. Shen, C.Y. Ragasa, Antimicrobial isothiocyanates from the seeds of *Moringa oleifera* Lam, Z. Naturforsch., C: J. Biosci. 67 (2012) 557–564, https://doi.org/10.1515/znc-2012-11-1205.
[17] J.M.P. Novitarini, D. Marlina, Antibacterial activity of Moringa plants (*Moringa oleifera* Lam.) to overcome antibiotic resistance: a systematic review, BioSci Med J Biomed Transl Res 1 (6) (2022) 2259–2273, https://doi.org/10.37275/bsm.v6i10.591.
[18] F. Anwar, S. Latif, M. Ashraf, A.H. Gilani, Moringa oleifera: a food plant with multiple medicinal uses, Phytother Res. 21 (2007) 17–25, https://doi.org/10.1002/ptr.2023.
[19] E. Camilleri, R. Blundell, A comprehensive review of the phytochemicals, health benefits, pharmacological safety and medicinal prospects of *Moringa oleifera*, Heliyon 10 (2024) e27807, https://doi.org/10.1016/j.heliyon.2024.e27807.
[20] S. Giacoppo, M. Galuppo, G.R. De Nicola, R. Iori, P. Bramanti, E. Mazzon, 4(α-l-Rhamnosyloxy)-benzyl isothiocyanate, a bioactive phytochemical that attenuates secondary damage in an experimental model of spinal cord injury, Bioorg. Med. Chem. 23 (2015) 80–88, https://doi.org/10.1016/j.bmc.2014.11.022.
[21] M.S. Jaafaru, N. Nordin, K. Shaari, R. Rosli, A.F. Abdull Razis, Isothiocyanate from *Moringa oleifera* seeds mitigates hydrogen peroxide-induced cytotoxicity and preserved morphological features of human neuronal cells, PLoS One 13 (2018) e0196403, https://doi.org/10.1371/journal.pone.0196403.
[22] M.S. Jaafaru, N. Nordin, R. Rosli, K. Shaari, H.Y. Bako, N.M. Noor, A.F. Abdull Razis, Prospective role of mitochondrial apoptotic pathway in mediating GMG-ITC to reduce cytotoxicity in H2O2-induced oxidative stress in differentiated SH-SY5Y cells, Biomed. Pharmacother. 119 (2019) 109445, https://doi.org/10.1016/j.biopha.2019.109445.
[23] S. Rim Jeon, K. Ha Lee, D. Ha Shin, S. Sang Kwon, J. Sung Hwang, Synergistic antimicrobial efficacy of mesoporous ZnO loaded with 4-(α-L-rhamnosyloxy)-benzyl isothiocyanate isolated from the *Moringa oleifera* seed, J. Gen. Appl. Microbiol. 60 (2014) 251–255, https://doi.org/10.2323/jgam.60.251.
[24] G. Deepika, S. Subbarayadu, A. Chaudhary, P.V.G.K. Sarma, Dibenzyl (benzo [d] thiazol-2-yl (hydroxy) methyl) phosphonate (DBTMP) showing anti-*S. aureus* and anti-biofilm properties by elevating activities of serine protease (SspA) and cysteine protease staphopain B (SspB), Arch. Microbiol. 204 (2022) 397, https://doi.org/10.1007/s00203-022-02974-y.
[25] K. Kitadokoro, M. Tanaka, T. Hikima, Y. Okuno, M. Yamamoto, S. Kamitani, Crystal structure of pathogenic *Staphylococcus aureus* lipase complex with the anti-obesity drug orlistat, Sci. Rep. 10 (2020) 5469, https://doi.org/10.1038/s41598-020-62427-8.
[26] C. Jianu, D. Stoin, I. Cocan, I. David, G. Pop, A.T. Lukinich-Gruia, M. Mioc, A. Mioc, C. Şoica, D. Muntean, L.-C. Rusu, I. Goleț, D.I. Horhat, *In silico* and *in vitro* evaluation of the antimicrobial and antioxidant potential of mentha × smithiana R. GRAHAM essential oil from western Romania, Foods 10 (2021) 815, https://doi.org/10.3390/foods10040815.
[27] H. Lade, J.-S. Kim, Bacterial targets of antibiotics in methicillin-resistant *Staphylococcus aureus*, Antibiotics 10 (2021) 398, https://doi.org/10.3390/antibiotics10040398.
[28] A. Dönhöfer, S. Franckenberg, S. Wickles, O. Berninghausen, R. Beckmann, D. N. Wilson, Structural basis for TetM-mediated tetracycline resistance, Proc. Natl. Acad. Sci. U.S.A. 109 (2012) 16900–16905, https://doi.org/10.1073/pnas.1208037109.
[29] A. Aleksandrov, L. Schuldt, W. Hinrichs, T. Simonson, Tetracycline-tet repressor binding specificity: insights from experiments and simulations, Biophys. J. 97 (2009) 2829–2838, https://doi.org/10.1016/j.bpj.2009.08.050.
[30] M. Kumaraswami, J.T. Schuman, S.M. Seo, G.W. Kaatz, R.G. Brennan, Structural and biochemical characterization of MepR, a multi-drug binding transcription regulator of the *Staphylococcus aureus* multi-drug efflux pump MepA, Nucleic Acids Res. 37 (2009) 1211–1224, https://doi.org/10.1093/nar/gkn1046.
[31] D. Meziane-Cherif, F.A. Saul, C. Moubareck, P. Weber, A. Haouz, P. Courvalin, B. Périchon, Molecular basis of vancomycin dependence in VanA-type *Staphylococcus aureus* VRSA-9-9, J. Bacteriol. 192 (2010) 5465–5471, https://doi.org/10.1128/JB.00613-10.
[32] W.S. Shehab, M.A. Aziz, N.K.R. Elhoseni, M.G. Assy, M.H. Abdellattif, E.O. Hamed, Design, synthesis, molecular docking, and evaluation antioxidant and antimicrobial activities for novel 3-phenylimidazolidin-4-one and 2-aminothiazol-4-one derivatives, Molecules 27 (2022) 767, https://doi.org/10.3390/molecules27030767.
[33] J.A.H.M. Bittencourt, M.F.A. Neto, P.S. Lacerda, R.C.V.S. Bittencourt, R.C. Silva, C. C. Lobato, L.B. Silva, F.H.A. Leite, J.P. Zuliani, J.M.C. Rosa, R.S. Borges, C.B. R. Santos, *In silico* evaluation of ibuprofen and two benzoylpropionic acid derivatives with potential anti-inflammatory activity, Molecules 24 (2019) 1476, https://doi.org/10.3390/molecules24081476.
[34] N. Pandit, R.K. Singla, B. Shrivastava, Current updates on oxazolidinone and its significance, Int J Med Chem 2012 (2012) 159285, https://doi.org/10.1155/2012/159285.
[35] N. Gupta, S. Bhattacharya, K. Urbanová, A. Dutta, A.K. Hazra, E. Fernández-Cusimamani, O. Leuner, Systematic analysis of antimicrobial activity, phytochemistry, and in silico molecular interaction of selected essential oils and their formulations from different Indian spices against foodborne bacteria, Heliyon 9 (2023) e22480, https://doi.org/10.1016/j.heliyon.2023.e22480.
[36] N.T. Tzvetkov, M.I. Peeva, M.G. Georgieva, V. Deneva, A.A. Balacheva, I. P. Bogdanov, M. Ponticelli, L. Milella, K. Kirilov, M. Matin, H.-G. Stammler, A. G. Atanasov, L. Antonov, Favipiravir vs. deferiprone: tautomeric, photophysical, in vitro biological studies, and binding interactions with SARS-Cov-2-M^{pro}/ACE2, Curr. Res. Biotechnol. 7 (2024) 100176.
[37] I. Reulecke, G. Lange, J. Albrecht, R. Klein, M. Rarey, Towards an integrated description of hydrogen bonding and dehydration: decreasing false positives in virtual screening with the HYDE scoring function, ChemMedChem 3 (6) (2008) 885–897. Schneider, N., Hindle, S., Lange, G., Klein, R., Albrecht, J., Briem, H., Beyer, K., Claußen, H., Gastreich, M., Lemmen, C., Rarey, M., 2012. Substantial improvements in large-scale redocking and screening using the novel HYDE scoring function. J. Comput.-Aided Mol. Des. 12, 701–723, and references therein.
[38] L. Wang, C. Ma, P. Wipf, H. Liu, W. Su, X.-Q. Xie, TargetHunter: an *in silico* target identification tool for predicting therapeutic potential of small organic molecules based on chemogenomic database, AAPS J. 15 (2013) 395–406, https://doi.org/10.1208/s12248-012-9449-z.

[39] A. Daina, O. Michielin, V. Zoete, SwissADME: a free web tool to evaluate pharmacokinetics, drug-likeness and medicinal chemistry friendliness of small molecules, Sci. Rep. 7 (2017) 42717, https://doi.org/10.1038/srep42717.
[40] M.A. Sirover, New insights into an old protein: the functional diversity of mammalian glyceraldehyde-3-phosphate dehydrogenase, Biochim. Biophys. Acta Protein Struct. Mol. Enzymol. 1432 (1999) 159–184, https://doi.org/10.1016/S0167-4838(99)00119-3.
[41] J. Liu, X. Zhou, R. Cai, D. Wu, Y. Bai, Exploring the active components and potential mechanisms of Qingre Liangxue Decoction in the treatment of psoriasis vulgaris with blood-heat syndrome based on UHPLC-Q-exactive Orbitrap/MS and network pharmacology, Res Square preprint (2024), https://doi.org/10.21203/rs.3.rs-3806518/v1.
[42] V. Bodnár, K. Antal, R.P. de Vries, I. Pócsi, T. Emri, *Aspergillus nidulans* gfdB, encoding the hyperosmotic stress protein glycerol-3-phosphate dehydrogenase, disrupts osmoadaptation in *Aspergillus wentii*, J Fungi 10 (2024) 291, https://doi.org/10.3390/jof10040291.
[43] G. Di Leo, F. Sardanelli, Statistical significance: p value, 0.05 threshold, and applications to radiomics—reasons for a conservative approach, Eur Radiol Exp 4 (2020) 18, https://doi.org/10.1186/s41747-020-0145-y.
[44] T.W. Johnson, R.A. Gallego, M.P. Edwards, Lipophilic Efficiency as an important metric in drug design, J. Med. Chem. 61 (2018) 6401–6420.
[45] A. Chandra, M. Chaudhary, I. Qamar, N. Singh, V. Nain, *In silico* identification and validation of natural antiviral compounds as potential inhibitors of SARS-CoV-2 methyltransferase, J. Biomol. Struct. Dyn. (n.d.) 1–11. https://doi.org/10.1080/07391102.2021.1886174.
[46] S. Saha, R. Nandi, P. Vishwakarma, A. Prakash, D. Kumar, Discovering potential RNA dependent RNA polymerase inhibitors as prospective drugs against COVID-19: an *in silico* approach, Front. Pharmacol. 12 (2021), https://doi.org/10.3389/fphar.2021.634047.
[47] D. Bhowmik, R. Nandi, R. Jagadeesan, N. Kumar, A. Prakash, D. Kumar, Identification of potential inhibitors against SARS-CoV-2 by targeting proteins responsible for envelope formation and virion assembly using docking based virtual screening, and pharmacokinetics approaches, Infect. Genet. Evol. 84 (2020) 104451, https://doi.org/10.1016/j.meegid.2020.104451.
[48] D.A. Abdelrheem, A.A. Rahman, K.N.M. Elsayed, H.R. Abd El-Mageed, H. S. Mohamed, S.A. Ahmed, Isolation, characterization, in vitro anticancer activity, dft calculations, molecular docking, bioactivity score, drug-likeness and admet studies of eight phytoconstituents from brown alga *sargassum platycarpum*, J. Mol. Struct. 1225 (2021) 129245, https://doi.org/10.1016/j.molstruc.2020.129245.
[49] Y.C. Martin, A bioavailability score, J. Med. Chem. 48 (2005) 3164–3170, https://doi.org/10.1021/jm0492002.
[50] C. Waterman, P. Rojas-Silva, T.B. Tumer, P. Kuhn, A.J. Richard, S. Wicks, J. M. Stephens, Z. Wang, R. Mynatt, W. Cefalu, I. Raskin, Isothiocyanate-rich *Moringa oleifera* extract reduces weight gain, insulin resistance, and hepatic gluconeogenesis in mice, Mol. Nutr. Food Res. 59 (2015) 1013–1024, https://doi.org/10.1002/mnfr.201400679.
[51] M. Galuppo, G.R.D. Nicola, R. Iori, P. Dell'Utri, P. Bramanti, E. Mazzon, Antibacterial activity of glucomoringin bioactivated with myrosinase against two important pathogens affecting the health of long-term patients in hospitals, Molecules 18 (2013) 14340–14348, https://doi.org/10.3390/molecules181114340.
[52] M.-A.W. Shalaby, E.M.E. Dokla, RabahA.T. Serya, K.A.M. Abouzid, Penicillin binding protein 2a: an overview and a medicinal chemistry perspective, Eur. J. Med. Chem. 199 (2020) 112312, https://doi.org/10.1016/j.ejmech.2020.112312.
[53] C.-O. Stiller, P. Hjemdahl, Lessons from 20 years with COX-2 inhibitors: importance of dose–response considerations and fair play in comparative trials, J. Intern. Med. 292 (2022) 557–574, https://doi.org/10.1111/joim.13505.
[54] M. Galuppo, S. Giacoppo, G.R. De Nicola, R. Iori, M. Navarra, G.E. Lombardo, P. Bramanti, E. Mazzon, Anti-inflammatory activity of glucomoringin isothiocyanate in a mouse model of experimental autoimmune encephalomyelitis, Fitoterapia 95 (2014) 160–174, https://doi.org/10.1016/j.fitote.2014.03.018.
[55] M.S. Jaafaru, N.A. Abd Karim, E. Mohamed Eliaser, P. Maitalata Waziri, H. Ahmed, M. Mustapha Barau, L. Kong, A.F. Abdull Razis, Nontoxic glucomoringin-isothiocyanate (GMG-ITC) rich soluble extract induces apoptosis and inhibits proliferation of human prostate adenocarcinoma cells (PC-3), Nutrients 10 (2018) 1174, https://doi.org/10.3390/nu10091174.
[56] A. Cipriano, M. Viviano, A. Feoli, C. Milite, G. Sarno, S. Castellano, G. Sbardella, NADPH oxidases: from molecular mechanisms to current inhibitors, J. Med. Chem. 66 (2023) 11632–11655, https://doi.org/10.1021/acs.jmedchem.3c00770.
[57] T.B. Tumer, P. Rojas-Silva, A. Poulev, I. Raskin, C. Waterman, Direct and indirect antioxidant activity of polyphenol- and isothiocyanate-enriched fractions from *Moringa oleifera*, J. Agric. Food Chem. 63 (2015) 1505–1513, https://doi.org/10.1021/jf505014n.
[58] D. Dahlgren, H. Lennernäs, Intestinal permeability and drug absorption: predictive experimental, computational and in vivo approaches, Pharmaceutics 11 (2019) 411, https://doi.org/10.3390/pharmaceutics11080411.
[59] A.L. Clutterbuck, K.E. Asplin, P. Harris, D. Allaway, A. Mobasheri, Targeting matrix metalloproteinases in inflammatory conditions, Curr. Drug Targets 10 (2009) 1245–1254, https://doi.org/10.2174/138945009789753264.
[60] Q. Wang, Y. Bao, Nanodelivery of natural isothiocyanates as a cancer therapeutic, Free Radic. Biol. Med. 167 (2021) 125–140, https://doi.org/10.1016/j.freeradbiomed.2021.02.044.
[61] W.S. Park, J. Lee, G. Na, S. Park, S.-K. Seo, J.S. Choi, W.-K. Jung, I.-W. Choi, Benzyl isothiocyanate attenuates inflammasome activation in *Pseudomonas aeruginosa* LPS-stimulated THP-1 cells and exerts regulation through the MAPKs/NF-κB pathway, Int. J. Mol. Sci. 23 (2022) 1228, https://doi.org/10.3390/ijms23031228.
[62] M. Richter, N. Vidovic, K. Biber, A. Dolga, C. Culmsee, R. Dodel, The neuroprotective role of microglial cells against amyloid beta-mediated toxicity in organotypic hippocampal slice cultures, Brain Pathol. 30 (2020) 589–602, https://doi.org/10.1111/bpa.12807.
[63] A. Ghasemi, J. Saeidi, M. Azimi-Nejad, S.I. Hashemy, Leptin-induced signaling pathways in cancer cell migration and invasion, Cell. Oncol. 42 (2019) 243–260, https://doi.org/10.1007/s13402-019-00428-0.
[64] S.R. Bahoosh, Y. Shokoohinia, M. Eftekhari, Glucosinolates and their hydrolysis products as potential nutraceuticals to combat cytokine storm in SARS-COV-2, DARU J Pharm Sci 30 (2022) 245–252, https://doi.org/10.1007/s40199-022-00435-x.
[65] C. Mallick, M. Mishra, V. Asati, V. Kashaw, R. Das, S.K. Kashaw, In silico-based structural prediction, molecular docking and ADMET analysis of novel imidazo-quinoline derivatives as pf purine nucleoside phosphorylase inhibitors, Curr. Signal Transduct. Ther. 18 (2023) 24–53, https://doi.org/10.2174/1574362418666221130164014.
[66] C. Mallick, M. Mishra, V. Asati, V. Kashaw, R. Das, A.K. Iyer, S.K. Kashaw, Integrated computational analysis on some indolo-quinoline derivatives for the development of novel antiplasmodium agents: CoMFA, pharmacophore mapping, molecular docking and ADMET studies, Curr. Signal Transduct. Ther. 17 (2022) 12–58, https://doi.org/10.2174/1574362416666210906155929.
[67] M.M. Mijwil, R. Doshi, K.K. Hiran, O.J. Unogwu, I. Bala, MobileNetV1-Based deep learning model for accurate brain tumor classification, Mesopotamian J. Comput. Sci. 2023 (2023) 29–38, https://doi.org/10.58496/MJCSC/2023/005.
[68] B. Maayah, A. Moussaoui, S. Bushnaq, O.A. Arqub, The multistep Laplace optimized decomposition method for solving fractional-order coronavirus disease model (COVID-19) via the Caputo fractional approach, Demonstr, Mathesis 55 (2022) 963–977, https://doi.org/10.1515/dema-2022-0183.
[69] M.O. Arowolo, M.O. Adebiyi, A.A. Adebiyi, O. Olugbara, Optimized hybrid investigative based dimensionality reduction methods for malaria vector using KNN classifier, J. Big Data 8 (2021) 29, https://doi.org/10.1186/s40537-021-00415-z.